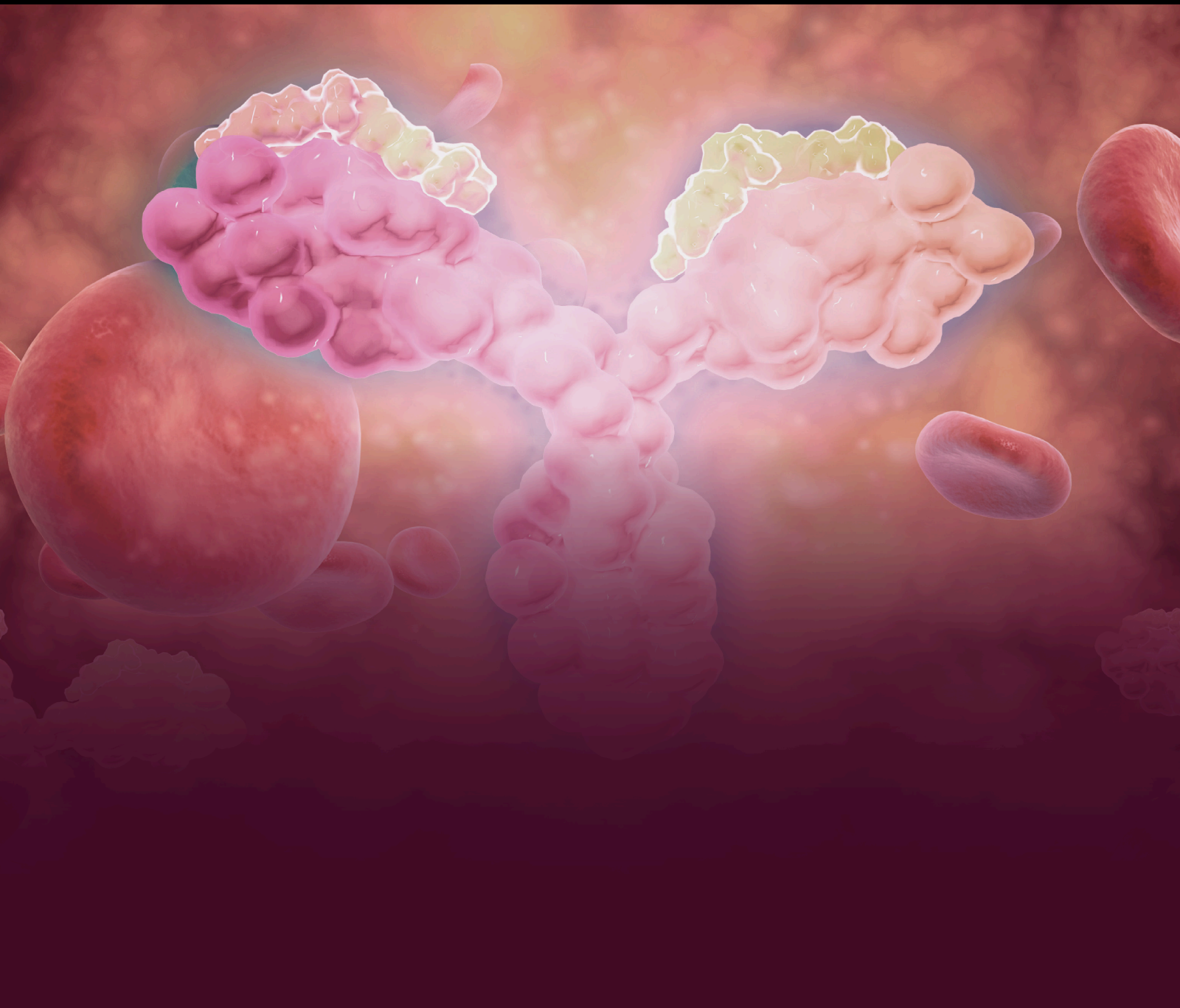


Viral Vectors and their Application in Treating Inherited Diseases

Lead Guest Editor: Dao Pan

Guest Editors: Nikunj Somia, Jim Vadolas, and Weidong Xiao





Viral Vectors and their Application in Treating Inherited Diseases

Advances in Cell and Gene Therapy

Viral Vectors and their Application in Treating Inherited Diseases

Lead Guest Editor: Dao Pan

Guest Editors: Nikunj Somia, Jim Vadolas, and Weidong Xiao



Copyright © 2023 Hindawi Limited. All rights reserved.

This is a special issue published in "Advances in Cell and Gene Therapy" All articles are open access articles distributed under the Creative Commons Attribution License, which permits unrestricted use, distribution, and reproduction in any medium, provided the original work is properly cited.

Chief Editor

Carol Miao , USA

Academic Editors

Wing Leung, Hong Kong



Dao Pan , USA

Weidong Xiao , USA



Advisory Board Member(s)

Contents

Comprehensive Comparison of AAV Purification Methods: Iodixanol Gradient Centrifugation vs. Immuno-Affinity Chromatography




Anh K. Lam , Patrick L. Mulcrone , Dylan Frabutt, Junping Zhang, Matthew Chrzanowski, Sreevani Arisa, Maite Munoz, Xin Li, Moanaro Biswas, David Markusic, Roland W. Herzog, and Weidong Xiao 
Research Article (12 pages), Article ID 2339702, Volume 2023 (2023)

Intra-Articular AAV9 α -L-Iduronidase Gene Replacement in the Canine Model of Mucopolysaccharidosis Type I

Raymond Yu-Jeang Wang , Shih-Hsin Kan , Haoyue Zhang, Jodi D. Smith , Afshin Aminian, Elizabeth Snella , Jackie K. Jens, Sarah P. Young, Patricia I. Dickson, and N. Matthew Ellinwood 
Research Article (14 pages), Article ID 7419017, Volume 2023 (2023)

Research Article

Comprehensive Comparison of AAV Purification Methods: Iodixanol Gradient Centrifugation vs. Immuno-Affinity Chromatography

Anh K. Lam ¹, Patrick L. Mulcrone ¹, Dylan Frabutt,¹ Junping Zhang,¹ Matthew Chrzanowski,² Sreevani Arisa,¹ Maite Munoz,¹ Xin Li,¹ Moanaro Biswas,¹ David Markusic,¹ Roland W. Herzog,¹ and Weidong Xiao ¹

¹Department of Pediatrics, Herman B Wells Center for Pediatric Research, Indiana University School of Medicine, Indianapolis, IN 46202, USA

²Lewis Katz School of Medicine, Temple University, Philadelphia, PA 19140, USA

Correspondence should be addressed to Weidong Xiao; xiaow@iu.edu

Received 18 April 2023; Revised 16 October 2023; Accepted 10 November 2023; Published 11 December 2023

Academic Editor: Loree Heller

Copyright © 2023 Anh K. Lam et al. This is an open access article distributed under the Creative Commons Attribution License, which permits unrestricted use, distribution, and reproduction in any medium, provided the original work is properly cited.

Recombinant adeno-associated viruses (AAVs) have emerged as a widely used gene delivery platform for both basic research and human gene therapy. To ensure and improve the safety profile of AAV vectors, substantial efforts have been dedicated to the vector production process development using suspension HEK293 cells. Here, we studied and compared two downstream purification methods, iodixanol gradient ultracentrifugation versus immuno-affinity chromatography (POROS™ CaptureSelect™ AAVX column). We tested multiple vector batches that were separately produced (including AAV5, AAV8, and AAV9 serotypes). To account for batch-to-batch variability, each batch was halved for subsequent purification by either iodixanol gradient centrifugation or affinity chromatography. In parallel, purified vectors were characterized, and transduction was compared both *in vitro* and *in vivo* in mice (using multiple transgenes: Gaussia luciferase, eGFP, and human factor IX). Each purification method was found to have its own advantages and disadvantages regarding purity, viral genome (vg) recovery, and relative empty particle content. Differences in transduction efficiency were found to reflect batch-to-batch variability rather than disparities between the two purification methods, which were similarly capable of yielding potent AAV vectors.

1. Introduction

Gene therapeutic agents are having a major, positive impact on researching and treating various diseases. Viral vector-based gene therapies are among the most efficient approaches for the correction of genetic defects. Among these, adeno-associated viruses (AAV) are most widely used for *in vivo* gene transfer, which is reflected in the five current FDA-approved AAV therapeutics for distinct genetic disorders: HEMGENIX [1] (AAV5, hemophilia B), ZOLGENSMA [2] (AAV9, spinal muscular atrophy), LUXTURN A [3] (AAV2, retinal dystrophy), ROCTAVIAN (AAV5, hemophilia A), and ELEVIDYS (AAVrh74, Duchenne muscular dystrophy). Towards clinical approval, translational

studies and preclinical studies require a high concentration of AAV titers to enable testing of design specifications, efficacy, side effects, and outcomes of the AAV gene transfer. To achieve the large quantities of vector required for such studies, production is scaled up by growing and transfecting suitable cells, such as human embryonic kidney cells (HEK293), in roller bottles, through continuous perfusion, or in WAVE Bioreactors [4]. Naturally, these scale-up processes result in not only larger amounts of the desired AAV but also of possible contaminants such as cellular proteins, membrane components, nucleic acid fragments, and empty capsid AAV particles. Therefore, purification of the AAV drug product is essential prior to carrying out translational and efficacy studies.

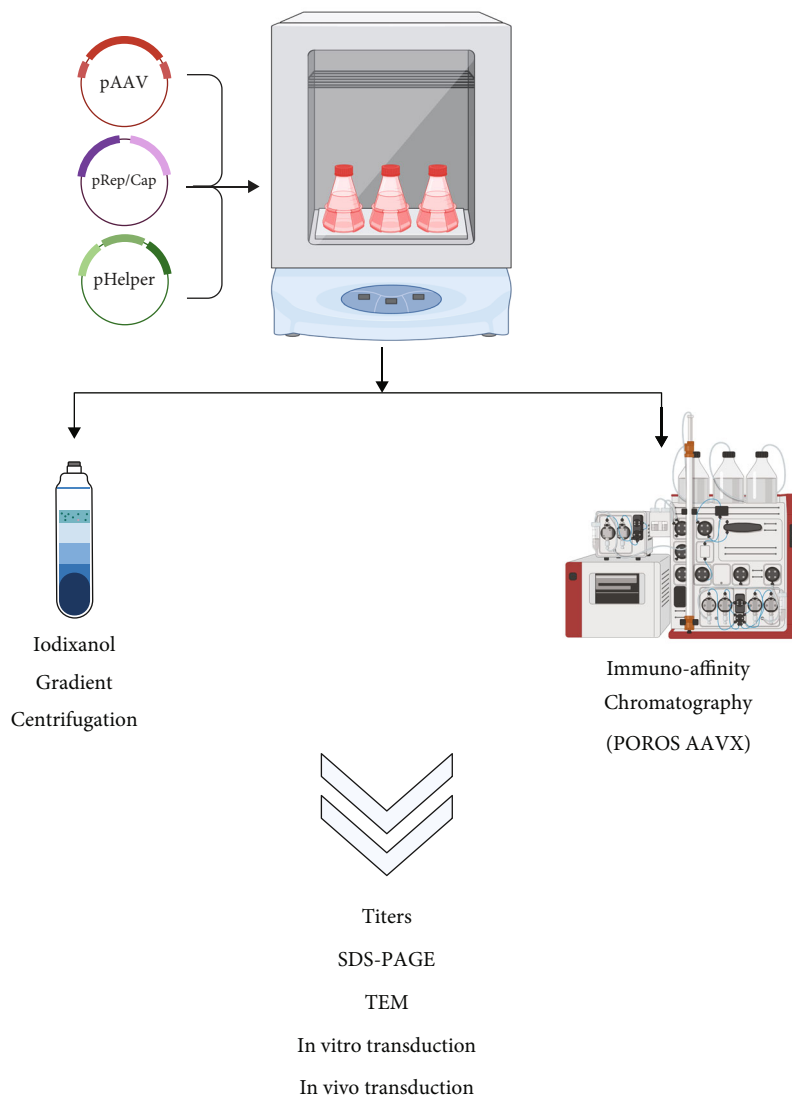


FIGURE 1: Schematic diagram of the AAV purification comparison study. Suspension HEK293 cells in orbital shake flasks were used to produce recombinant AAVs by the triple-plasmid transfection method. Each batch was split in half for subsequent purification by either iodixanol gradient centrifugation or immune-affinity chromatography (POROS™ CaptureSelect™ AAVX column). The resulting vectors were then studied and characterized by both *in vitro* and *in vivo* assays.

The two most conventional methods for AAV purification are cesium chloride (CsCl) and iodixanol gradient ultracentrifugation (IOD), which separate particles based on their buoyant density or sedimentation rates. These methods are independent of capsid serotypes and allow the separation of empty and full virions. Because the CsCl-based method is time-consuming and may introduce toxicity, iodixanol has become a more preferred method [5]. For a more scalable process, column chromatography is well established and has been adapted for AAV purification [6, 7]. Immuno-affinity chromatography specifically utilizes an affinity-binding interaction between the column resin and the desired product to be purified. Clinical-grade AAV vectors have been reported to be purified using both methods of gradient centrifugation and column chromatography, or a combination of both, since the ultracentrifugation method is difficult to scale up [8–12]. Given the importance of the purification

methodology (under the CMC Guidance for Industry from the US FDA) [13], we compared two commonly used purification methods across various AAV serotypes to determine if biological differences *in vitro* and *in vivo* could be affected by a specific purification approach.

To avoid overinterpretation and batch-to-batch errors, separate lots of AAV vectors were produced and analyzed independently. In this study, we report comprehensive comparison data of three independent AAV batches (AAV5, AAV8, and AAV9) purified by one round of either iodixanol gradient centrifugation (IOD) or affinity chromatography using the POROS™ CaptureSelect™ AAVX column (POR). These data include characterizations of purity, the relative presence of empty capsids (SDS-PAGE and transmission electron microscopy), and titers and plasmid backbone contaminations (qPCR). Furthermore, transduction efficiencies were determined *in vitro* and *in vivo* (using self-

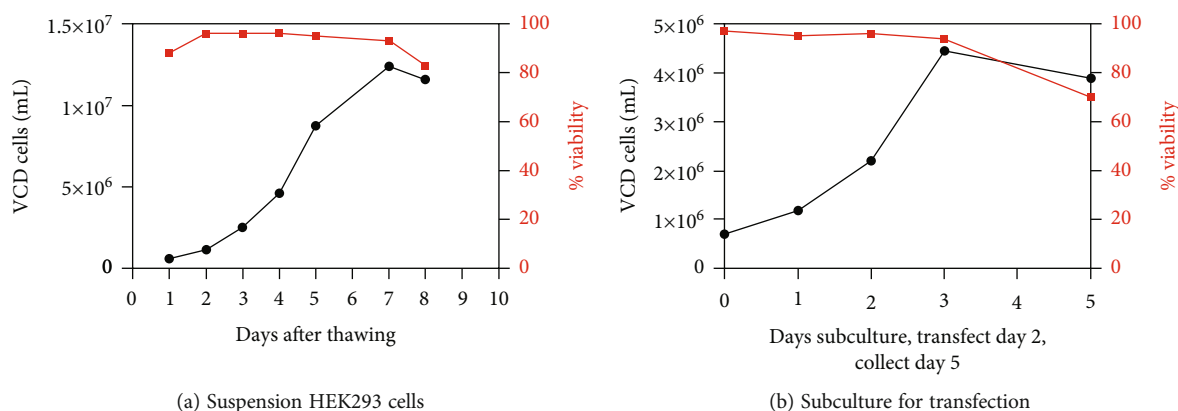


FIGURE 2: Viability and viable cell density (VCD) representation of scalable suspension system HEK293 cells: freshly thawed cells (a) and subcultured cells (b). Transfection was performed on day 2 with a VCD of $\sim 2.0\text{--}2.5 \times 10^6$ cells/mL and viability of $>92\%$ and vector harvest was at day 5, which was 72 hr posttransfection.

complementary AAV-CB-eGFP, AAV-CB-GLUC, and AAV-TTR-cohFIX constructs) as outlined in Figure 1.

2. Results

Orbital shake flasks for cell culture were used for a research scale of 125 mL–1000 mL (max 25% volume of cell culture). A suspension system of HEK293 cells was optimized so that on the day of transfection, the viable cell density (VCD) and % viability were ~ 2.0 to 2.5×10^6 cells/mL and $>92\%$, respectively (Figure 2).

At the time of vector harvest, 72 hrs posttransfection, the cells and media were collected and split in half for parallel purification by IOD or POR. For downstream analyses, purified vectors from both methods were side-by-side characterized, tittered, and transduced cells *in vitro* and IV-injected via the tail vein of mice for transgene expression comparison.

Multiple batches of AAVs including AAV5, AAV8, and AAV9 were characterized by SDS-PAGE to compare their relative purity. As shown in Figures 3(a) and 3(b), AAV vectors generated via the IOD method were often less pure and contaminated with other proteins, as detected by smears in addition to the three bands corresponding to VP1, 2, and 3. When normalized to the vg loaded per lane of SDS-PAGE, the POR method yielded approximately 2- to 5-fold more empty capsids compared to the IOD method, as indicated by the darker bands for VP1, 2, and 3 (Figure 3(b), estimate based on pixel contrast by ImageJ).

The titers of AAV vg recovered by both purification methods were found to be comparatively similar (Figure 3 (c)). Plasmid backbone contamination was also examined by using primers and probes that target ampicillin. As shown in Figure 3(d), pretreatment of DNase I prior to vg titration reduced the % of plasmid backbone contamination in both IOD and POR samples from $\sim 6.5\%$ to $\sim 5.7\%$, which could be from impurity DNA/plasmid fragments stuck on the capsids.

Images from TEM confirmed more impurities in IOD vectors as many patches of debris are observed surrounding

each virion, leading to poorer image quality (Figure 4(a)). One common impurity from the IOD purified vector appears as smaller circles (indicated by white arrows) which was identified by previous studies to be ferritin [14]. Greater purity was found in POR-purified vectors, but more empty capsids (80–90%, based on ImageJ counting of ~ 1000 particles) were seen in POR vectors (TEM images in Figure 4). This confirms the data from SDS-PAGE in Figure 3.

Transduction efficiency was determined *in vitro* by infecting human GM16095 fibroblast cells and quantifying gene expression after 48–72 hrs of AAV infection. Figure 5 (a) shows transduction efficiency by AAV5-CB-eGFP measured by flow cytometry as % GFP-positive cells and mean fluorescent intensity (MFI) signals. Despite the difference in empty capsids per group, the multiplicity of infection (MOI) was normalized based on vg content titrated by qPCR. At the same MOI of 100,000, IOD-purified AAV5 had significantly higher transduction efficiency than POR AAV5 ($\sim 90\%$ eGFP $>70\%$ eGFP positive), which indicated that the excess number of empty capsids detrimentally affects the transduction *in vitro*. However, *in vivo* testing demonstrated opposite results, as POR AAV5 trended to transduce the livers of WT BALB/c mice better than IOD AAV5, although this difference did not reach statistical significance (Figure 5(b)).

In another study using AAV8-CB-eGFP, an *in vitro* transduction assay showed the same trend, as IOD AAV8 outperformed POR AAV8 at the same MOI in GM16095 cells (Figure 6(a)). To determine the effect of empty capsids, we added an equivalent of virions (based on SDS-PAGE) without any packaged transgene to the same MOI of IOD AAV8 or POR AAV8; as a result, the transduced cells measured as % GFP positive were significantly decreased by the addition of empty capsids (Figure 6(a)). This indicated that empty capsids, *in vitro*, could potentially compete for the AAV trafficking machinery of the host cells and therefore lead to a decrease in transduction. *In vivo* data of liver transduction, measured at week 2 postinfection, provided no significant difference between IOD AAV8 and POR AAV8 in terms of % GFP-positive hepatocytes, while slightly higher

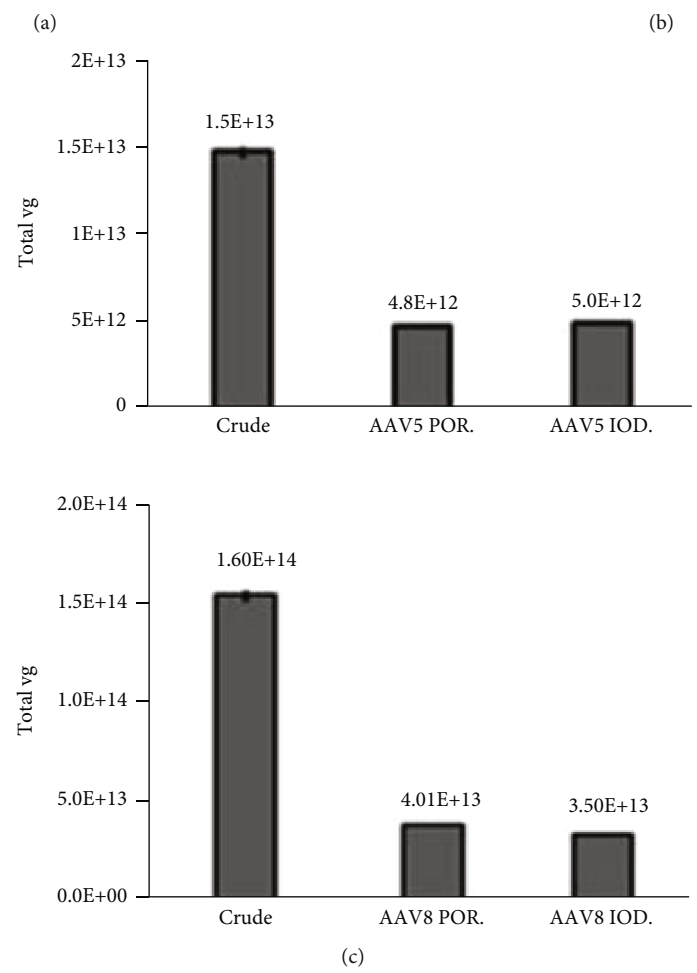
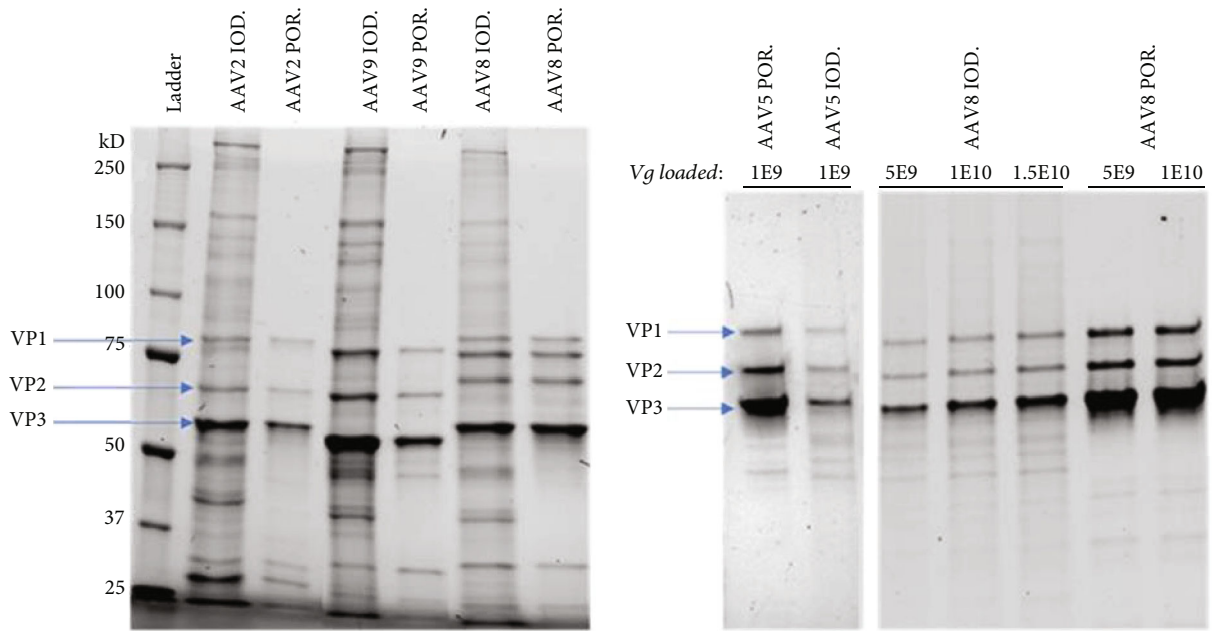


FIGURE 3: Continued.

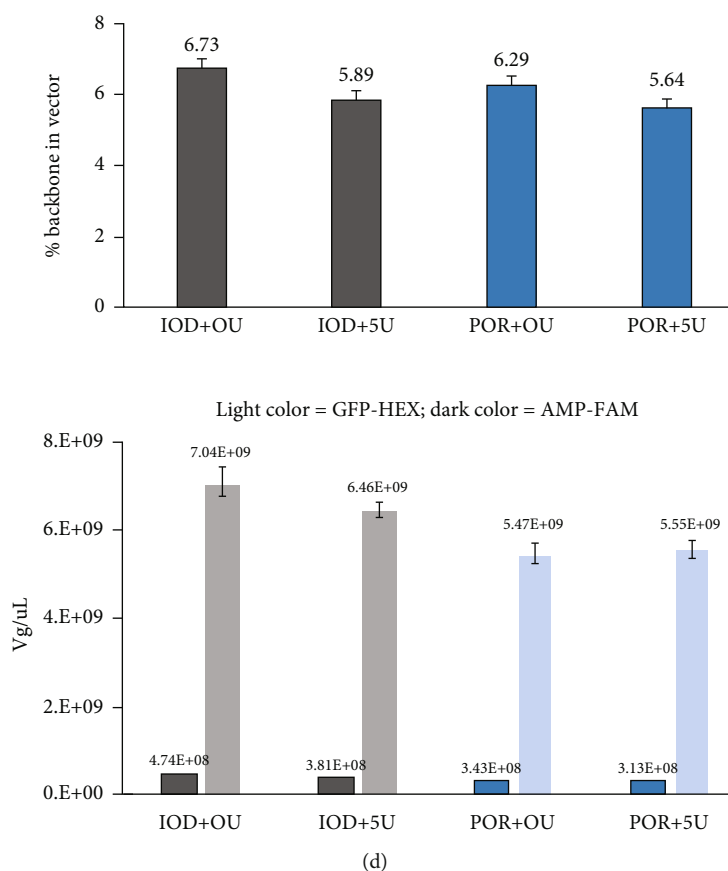


FIGURE 3: AAV vector genome and capsid protein characterization using SDS-PAGE (7.5% gel) and qPCR probe-based titration. POROS-AAVX affinity column purified (POR) vectors are purer than their iodixanol (IOD) purified counterparts (a). With the same titer of vg loaded, POR vectors show darker bands which indicate more empty capsids than IOD vectors (b). Using qPCR probe-based analysis, vg recovered by both purification methods are comparably similar ((c) top: from 50 mL of triple-plasmid-transfected cell culture; bottom: from 200 mL). Backbone contaminations were determined and multiplexed using an ampicillin-primers/probe, which indicated a similar amount of the plasmid backbone packaged by AAV8 purified by both methods (d). 0 U = no pretreatment of DNase I before qPCR titration; 5 U = 5 units of DNase I pretreatment were used prior to qPCR.

transduction was found by IOD AAV8 in terms of the GFP MFI signal (Figure 6(b)).

As shown in Figure 7, a serial dilution of empty capsids of AAV9 added to the same MOI of AAV9-CB-GLUC led to variable transduction outcomes. The addition of empty capsids did not detrimentally affect the infectivity of AAV9 when that percentage of empty capsids was under ~41% (Figures 7(a) and 7(b)), as the transduction readout of luminescence was not lower. When the amount of empty capsids added exceeds 100%, the standard deviation becomes broader, leading to a difficult conclusion. This result shows that *in vitro*, transduction efficiency may vary depending on how much empty capsids are present.

In the third batch of AAV, we produced AAV9-TTR-cohFIX, which is a codon-optimized construct encoding human factor IX (hFIX) for treating hemophilia B. The hemophilic B mouse model, C3H/HeJ-HB, was used to test the functionality of the differently purified vectors (Figure 8 (a)). At weeks 1, 5, and 8 post-IV injections of the AAV, we collected blood for hFIX ELISA. The efficacy was measured based on the amount of circulating hFIX. While no significant difference was found at week 1 postinjection, POR

AAV9 outperformed IOD AAV9 at week 5 and week 8 time points, yielding significantly ~2-fold higher hFIX levels (Figure 8(b)).

3. Discussion

The preparation and purification processes related to AAV production are essential for the sound interpretation of translational and preclinical investigations. As there are multiple methods to purify AAVs, it is imperative to research details related to how these processes affect different serotypes and batch preparations of AAVs. In this study, we report comprehensive comparison data from three self-complementary AAV serotype batches (AAV5, AAV8, and AAV9) prepared independently and purified by iodixanol gradient centrifugation (IOD) or affinity chromatography using the POROS™ CaptureSelect™ AAVX column (POR). These data include characterizations of purity, the relative empty capsid content (SDS-PAGE and transmission electron microscopy), titers of vg recovery, and plasmid backbone contaminations (qPCR). Our focus was to assess transduction efficiency *in vitro* and *in vivo* in WT mice plus

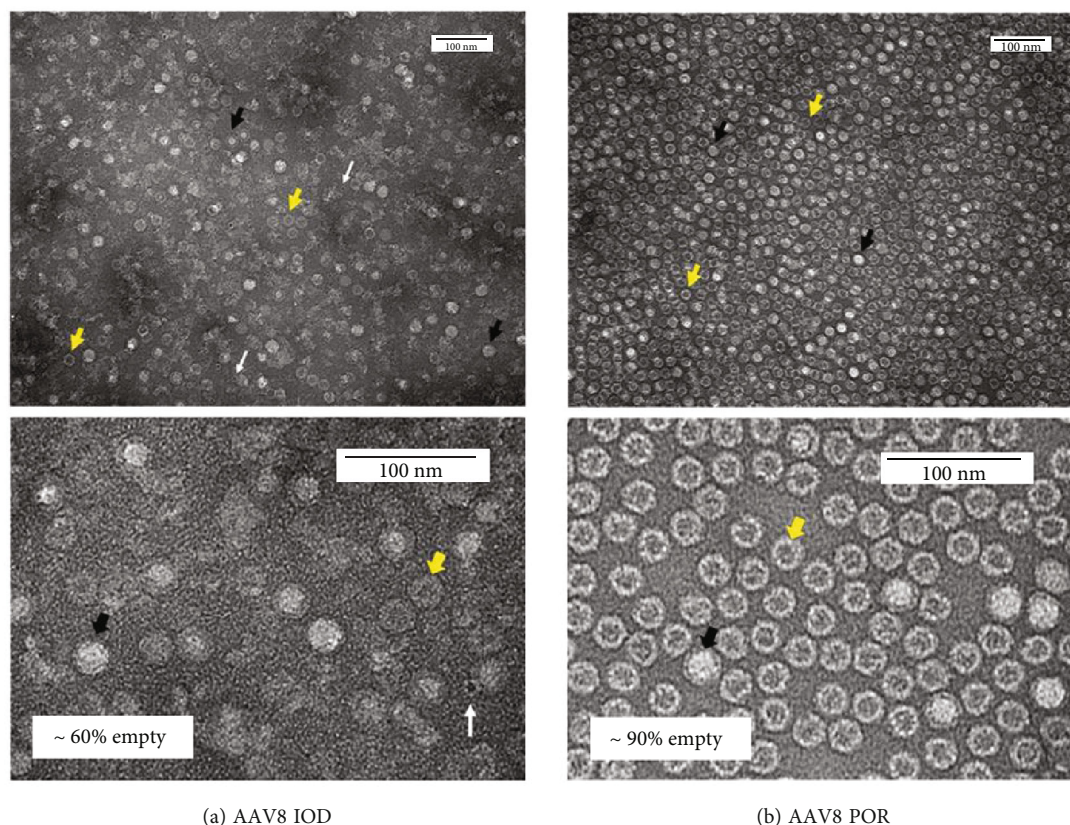


FIGURE 4: Transmission electron micrographs of AAV8 purified by iodixanol gradient centrifugation (a) or by POROS AAVX column (b). Both samples were imaged at 5E9 vg/ μ L with a negative stain. More impurities were identified from iodixanol gradient centrifugation (a) including ferritin, as indicated by white arrows, as identified by previous studies [14]. Empty capsids—indicated by yellow arrows—were observed as denser virions from affinity column purified vectors (b). The empty capsid amount was estimated and shown on the lower panels. Black arrows indicate full capsids; scale bars = 100 nm.

a clinically relevant model of hemophilia B (C3H/HEJ-HB mice), as designed in Figure 1.

In this study, we employed a scalable vector production system utilizing a suspension of HEK293 cells that were cultured and maintained at a viable cell density and percentage of viability, as shown in Figure 2. Each batch of vectors was halved for the IOD or POR purification approach, followed by further characterization and transduction efficiency analyses. One standout advantage of affinity column purification is improved consistency in the high-level purity of AAV products, while iodixanol gradient centrifugation often yields more impurities like ferritin and other host proteins (Figures 3(a) and 3(b) and 4). In contrast, the iodixanol gradient method can be implemented independently of the capsid serotype, while affinity chromatography is reported to be effective for certain wild-type serotypes. AAV empty capsids have been described to vary in different vector production systems, can comprise up to 90% of total AAV particles generated, and even within one production system, empty capsid content can fluctuate highly between manufacturing batches [15]. One limitation of our study is that no absolute quantification of empty capsids per method of purification was calculated. Nevertheless, as we observed from the TEM images and SDS-PAGE gels, the relative empty capsids in each batch of AAV product purified by POR were always

higher than those from IOD (Figures 3 and 4). Vector recovery (vg titer from qPCR) from both methods was comparable, as shown in Figure 3(c). Using a relative comparison of multiplexed qPCR, DNA impurities from plasmid backbones measured by ampicillin primers and probes were found to be ~6% by both purification methods (Figure 3 (d), dark color bars). Pretreatment of DNase I prior to qPCR titering reduced the DNA impurity by about 1%, which indicated that some of the plasmid backbones were present outside of the capsid and ~5% were packaged by the vector. Other studies have reported that this backbone contamination could be a result of defective virions (including single ITR and snapback genome vectors) and can be minimized by having a transgene size close to the maximum packaging capacity of the rAAV (~5 kb) [16, 17].

In vitro, POR AAV vectors were found to transduce GM16095 human fibroblasts less efficiently than their counterpart IOD AAVs (Figures 5(a) and 6(a)). One hypothesis was that the higher ratio of empty capsids in POR AAV preparations competes with the full particles for receptor binding on host cells and leads to lower gene expression. To test this hypothesis, we generated AAV9-CB-GLUC vectors spiked with different amounts of empty capsids (Figure 7). To detrimentally affect transduction efficacy, a large number of empty particles were required (greater than

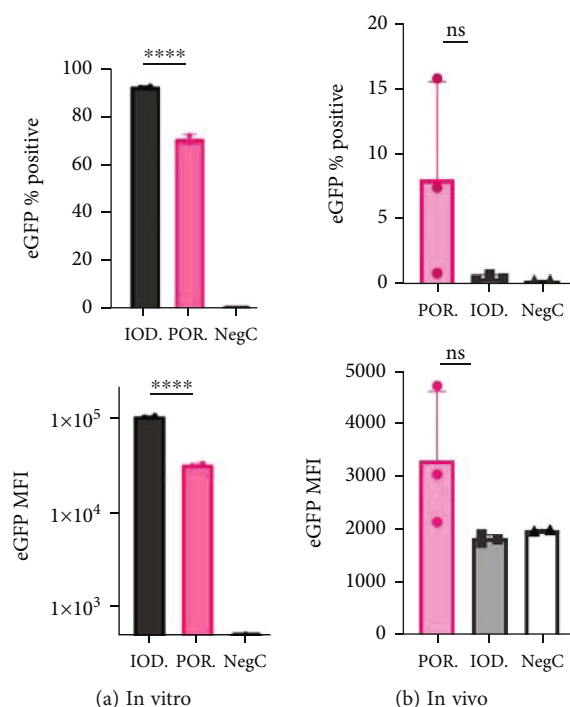


FIGURE 5: Transduction efficiency of AAV5-CB-eGFP measured by flow cytometry. *In vitro* transduction results of GM16095 cells ((a) MOI = 100 K; $n = 2$ wells/group). *In vivo* transduction results of WT BALB/c mouse livers at week 2 post-IV-injection ((b) $n = 3$ /group; dose = 1×10^{11} vg/mouse). A two-way ANOVA with Turkey's multiple comparisons was performed. MFI = mean fluorescence intensity; %eGFP positive = percent positive cells of eGFP. * $P < 0.05$, ** $P < 0.01$, *** $P < 0.001$, **** $P < 0.0001$.

41% empty capsids added to lower the LUM readout). However, the *in vivo* data for each batch did not fully corroborate the *in vitro* results. As shown in Figure 5(b), POR AAV5 yielded slightly higher gene expression of % GFP-positive cells compared to IOD AAV5 in the mouse liver at week 2 postinjection, although no significant statistical difference was found due to a large standard deviation. In contrast, Figure 6(b) shows that POR AAV8 yielded slightly lower gene expression of % GFP-positive liver cells as compared to IOD AAV8 in the mouse liver at week 2 postinjection. These mixed *in vivo* results between the two batches of AAV5 and AAV8 could be from the end-point analysis at week 2 PI because the gene expression delivered by different serotypes of AAV might require different times to be fully expressed. The third batch of AAV9-packaged codon-optimized human factor IX (hFIX) was added to the study to assess functional differences in the preparation methods in a clinically relevant disease model for AAV gene therapy. As shown in Figure 8 using a hemophilia B mouse model, no significant difference in hFIX was found in the plasma between IOD and POR AAV9 at week 1 PI. However, at week 5 and week 8 PI, plasma hFIX delivered by POR AAV9 was significantly higher than those delivered by the IOD AAV9, suggesting that a higher purity vector preparation (other than empty capsids) may be beneficial for *in vivo* gene delivery. There are several possible contributions to these disparate results between *in vitro* and *in vivo* transduction including impurities or a variety of empty capsids in each batch since we did not normalize the empty cap-

sid of each serotype for the *in vivo* experiments. Regardless, our data showed that vectors purified by affinity chromatography could successfully deliver the gene of interest in mice, if not better, compared to iodixanol gradient centrifugation, despite the higher content of empty capsids. In a previous study reported by Blessing et al. [18], intrastriatal injection in adult mice showed that AAV2/9 purified by the iodixanol gradient centrifugation method had significantly higher transduction than vector purified by the affinity POROS AAV column at week 4 postinjection. This could be due to the empty capsid content, batch-to-batch variation, or timing differences in their experiment compared to ours presented here.

While the iodixanol gradient can separate full and empty particles from one another, residual iodixanol in the final AAV product may pose a safety concern and may warrant additional purification steps. Pu et al. have reported an LCMS method for the detection of residual iodixanol [19]. As investigational AAV-based products continue to move through clinical development, more *in vivo* studies are needed to examine the impact of downstream processing of AAV vectors, particularly focusing on differences in the ratio of empty-to-full viral particles and impurities present in vector batches. Some clinical trials and preclinical studies intentionally mixed AAV empty capsids to act as decoys for neutralizing anti-AAV antibodies and therefore enhanced gene transfer [20]. In other cases, they were undesirable as they could elicit liver toxicity due to activation of CD8⁺ T cells and TLR2 [21–23]. Thus, studying how the systematic

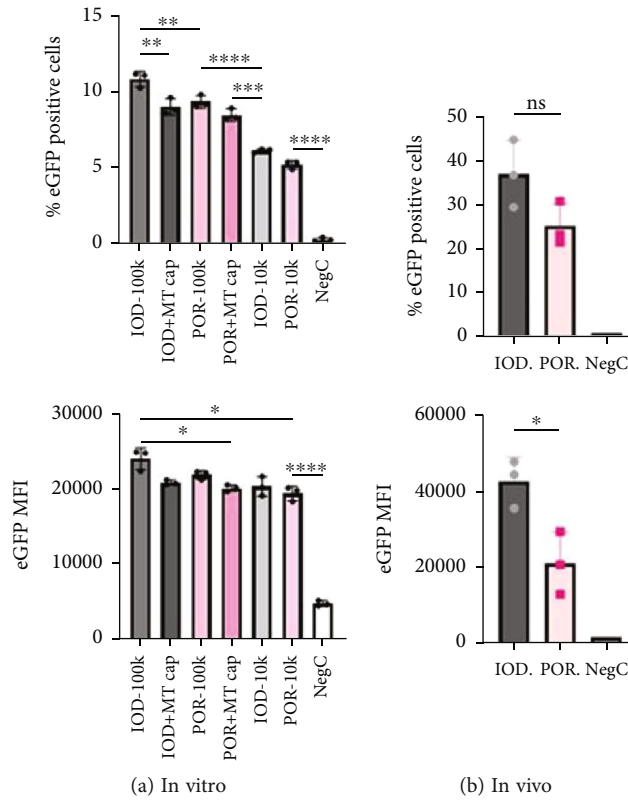


FIGURE 6: Transduction efficiency of AAV8-CB-eGFP measured by flow cytometry. *In vitro* transduction results of GM16095 cells ((a) MOI = 100 K or 10 K; $n = 3$ wells/group; MT cap = empty capsids). *In vivo* transduction results of WT BALB/c mouse livers at week 2 post-IV-injection ((b) $n = 3$ /group; dose = 2×10^{11} vg/mouse). A two-way ANOVA with Turkey’s multiple comparisons was performed. MFI = mean fluorescence intensity; %eGFP positive = percent positive cells of eGFP. * $P < 0.05$, ** $P < 0.01$, *** $P < 0.001$, **** $P < 0.0001$.

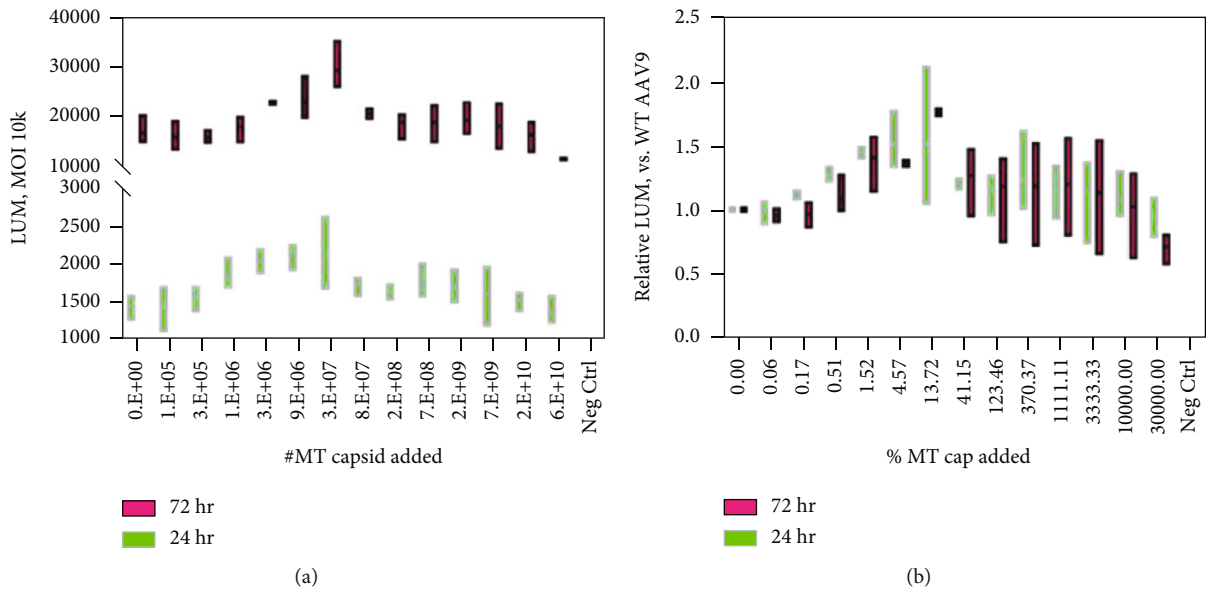


FIGURE 7: Transduction results of AAV9-CB-GLUC vs. empty capsids added on GM16095 cells. $N = 3$ wells/group. Luminometer readouts at 24 hrs (green) and 72 hrs (red) postinfection (a). Relative LUM readouts compared to WT AAV9 (b). MT cap = empty capsids.

addition of empty particles impacts the immune response is important to identify a threshold of empty capsid content that maximizes both safety and transduction efficacy. Given

the adverse side effects in multiple clinical trials of AAV-based drugs [24] and the less well-understood effects of impurities like empty capsids and residual plasmid DNA,

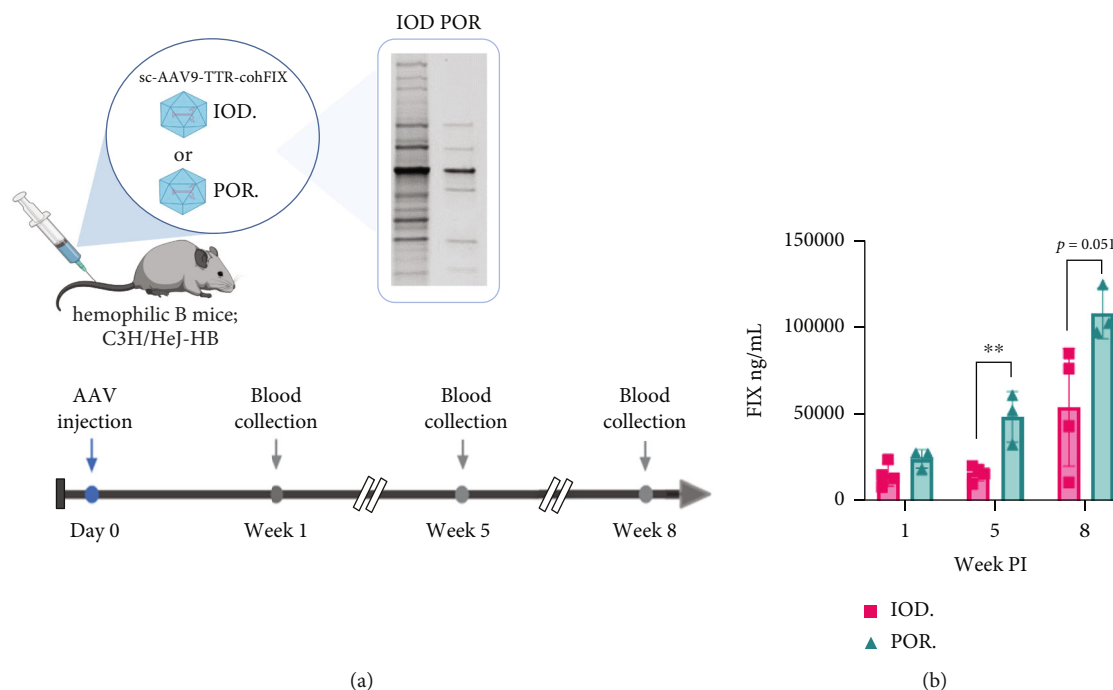


FIGURE 8: Comparison of systemic hFIX expression in hemophilia B mice. Study design with an inset of SDS-PAGE for purity comparison (a). Plasma level of hFIX in ng/mL (b). Dose = 1×10^{11} vg/mouse; $n = 3-4$ /group. No difference was found between the two purification methods found at week 1 PI, but weeks 5 and 8 showed a clearer difference in which POROS-AAVX purified AAV9 achieved better transduction efficacy compared to iodixanol purified AAV9. Two-tailed unpaired t -test, ** p value < 0.01.

TABLE 1: Comparative properties of iodixanol gradient centrifugation versus immuno-affinity chromatography.

	Iodixanol gradient centrifugation	Immuno-affinity chromatography
Purity	Poorer	Better
Yield monitor	No	Yes (A280 nm)
AAV serotypes	Independent	Depend on column type
Time-consuming	Yes (more steps: PEG precipitation)	Faster + automatic system
Impurities	Residual iodixanol & large proteins	Small proteins
Empty capsids	Less	More
Scalability	No	Yes
GMP readiness	Poor	Good

regulatory agencies have proposed risk mitigation plans that include the manufacturing process of AAV to decrease the percentage of empty capsids in 2021 [25]. Many studies have proposed chromatography methods to separate full and empty capsids using ion-exchanged columns based on the slight difference in charge possessed by the nucleic acid content of the full virions [5, 26–28].

Any physiochemical and biological properties (full-to-empty ratio, purification method, formulation excipients, phenotypic variation, capsid serotype, infectivity per dose per route of administration, etc.) should be well documented, even though the effects of these on vector performance might not be fully understood. With more knowledge about AAVs being documented, studied, and disseminated, detailed bookkeeping and certification on process development would be a valuable tool for risk mitigation to ensure the safety and well-being of patients in the clinic.

4. Conclusion

Neither the IOD nor POR purification method was found to be superior overall. Each purification method was found to have its own advantages and disadvantages (summarized in Table 1). *In vitro* data show that IOD-purified vectors outperformed POR-purified ones. Empty capsids were found to decrease the infectivity of AAVs *in vitro* at high concentration. However, *in vivo* data show variable results from batch-to-batch of different AAVs with no consistent trend. Titer normalization, purity, and types of impurities in a final AAV product may play a big component in determining vector potency. In conclusion, iodixanol gradient centrifugation and affinity chromatography have their own advantages and limitations, and both are similarly capable of yielding infectious AAV vectors for research scale. For manufacturing on a large scale, additional processes are needed to

minimize impurities in each batch for more consistent quality control of the final AAV product.

5. Materials and Methods

5.1. rAAV Production. The suspension cell line HEK293F was used for rAAV vector production. The cells were cultured in viral production medium (Thermo, Cat#A4817901) in shaker flasks at 120 rpm at 37°C, 8% CO₂. Cell viability was maintained at >95%, and transfection was performed when the cell density was at ~2-2.5E6 cells/mL using the standard triple-plasmid transfection method of pRep2CapX (X = serotype 5, 8, and 9), pHelper, and pITR-AAV (pds-CB-EGFP, CB-GLUC, or TTR-cohFIX) at an equal molar ratio, plus transfection agent Fectovir. For empty capsid production, no p-ITR-AAV was used. These cells were collected at 72 hr posttransfection. Centrifugation at 3000 g for 15 min was performed to separate the cells and media. The cells were resuspended in lysis buffer of 50 mM Tris-HCl (+0.15 M NaCl, pH 8.2), went through 3 cycles of freeze/thaw to release rAAV viruses, and centrifuged at 3000 g for 20 min to collect the supernatant. This supernatant was combined with the cell media and treated with DNase I (5 U/mL) for 1 hr at 37°C to digest contaminant DNAs and improve the quality of the crude lysate. The rAAV viruses in the crude were purified using either iodixanol gradient centrifugation or liquid chromatography with an affinity column (POROS AAVX CaptureSelect, Thermo #A36651).

5.2. rAAV Purifications. *Iodixanol gradient ultracentrifugation* followed the Addgene protocol using Option #3, puncturing the QuickSeal tube slightly below the 60-40% interface (<https://www.addgene.org/protocols/aav-purification-iodixanol-gradient-ultracentrifugation/>).

An *immuno-affinity chromatography* detailed protocol was reported by Lam et al. [29].

Briefly, the POROS™ CaptureSelect™ AAVX column was used with an AKTA GO system controlled by UNICORN 7.6 software. The equilibration and wash buffer were PBS, pH 7.2. The secondary wash buffer was 18% ethanol and PBS+1 M NaCl. The elution buffer was 0.05 M citric acid+0.1 M glycine+0.1% p188 (pH 2.9). Eluted fractions were neutralized by 1 M Tris-HCl buffer (pH 8.2), and then the buffer was exchanged with PBS and concentrated down using centrifugal Vivaspin, 20 mL, 100 K MWCO.

5.3. SDS-PAGE. Mini-PROTEAN TGX precast gel (7.5% polyacrylamide gel, Bio-Rad) was used. Samples plus Laemmli buffer containing 10% of β-mercaptoethanol were mixed and heated at 90°C for 5 min. The samples were cooled to room temperature and loaded into the gel lanes, together with a standard marker. The running buffer was 1 × Tris /glycine/SDS, Bio-Rad. The assembly was set and connected. The voltage was set to be constant at 200 V. The gel was set to electrophoresis for 30 min. The gel was removed from the cassette and imaged according to the manufacturer's protocol using a ChemiDoc MP Imaging System (Bio-Rad).

5.4. Transmission Electron Microscopy. Purified AAV samples (3 μL) were negative stained with NanoVan (3 μL) on

a nickel Formval/Carbon 300 mesh. The samples were air-dried before being imaged at 120 kV using a Tecnai Spirit equipped with an AMT CCD camera (Thermo Fisher).

5.5. In Vitro Cell Culture and Transduction Assays. GM16095 human fibroblast cells were purchased from the Coriell Institute and grown in 10% FBS DMEM with 1% antibiotics at 37°C with 5% CO₂. The cells were subcultured once they reached 90% confluency. For transduction assays, the cells were counted and seeded in a 96-well plate 24 hrs before transduction with rAAVs. Based on the AAV transgene of each experiment, the cells were trypsinized for flow cytometry to determine % GFP positive or measured for Gaussia luciferase activity (using the Pierce Gaussia Luciferase Glow Assay Kit, Thermo Fisher #16161, following the manufacturer's protocol).

5.6. Animal In Vivo Experiments. All mice were maintained in the laboratory animal resource center at Indiana University–Purdue University, Indianapolis (IUPUI). All animal experimental protocols were approved and performed as per the guidelines of Indiana University's Institutional Biosafety Committees (IBC) and Institutional Animal Care and Use Committee (IACUC). Each specific experiment (specified in each result figure) includes either WT BALB/c mice (purchased from the Jackson Lab) or hemophilia B C3H/HeJ-HB mice (in-house breed) [30]. All mice were treated with rAAVs (purified by either iodixanol centrifugation or affinity chromatography) at 8-10 weeks old; the negative control group was mock-injected with PBS. AAV dosage was 1E11 to 2E11 vg/mouse (see figure legends for details of each experiment). For the BALB/c mice, at sacrifice (week 2 postinjection), their livers were harvested for further flow cytometry analysis. For the C3H/HeJ-HB mice, plasma samples were collected by retroorbital eye bleed into 0.38% sodium citrate.

5.7. Flow Cytometry Analysis. Mouse livers were processed on the day of harvest and measured for eGFP signal based on a previously described protocol [31] with a slightly modified digestion step as follows: a single lobe was digested in 7 mL of digestion media (0.2 mg/mL collagenase P, 5 U/mL DNase I, 1.5 U/mL dispase, and 1% FBS in RPMI 1640). Simple gating for unfixed, single cells from the liver was set for direct fluorescence of GFP+ cells from negative control GFP cells using the Attune NxT Flow Cytometer.

5.8. hFIX ELISA. Enzyme-linked immunosorbent assay-(ELISA-) based measurements of human FIX from the mouse plasma were carried out as previously described [32].

5.9. Statistics. GraphPad Prism 9.1.2 software was used to calculate all statistics. Unless otherwise stated, data are presented as means ± standard deviations.

Data Availability

The datasets used and/or analyzed during the current study are available from the corresponding author on reasonable request.

Conflicts of Interest

The authors declare that they have no conflicts of interest.

Authors' Contributions

AKL provided substantial contributions to the conceptualization, methodology, validation, formal analysis, investigation, data curation, and writing. WX was responsible for the conceptualization, supervision, and funding acquisition. All other authors contributed to resources, data analyses, reviewing, and editing.

Funding

Dylan Frabutt is supported by the training grant 5T32HL007910-23.

Acknowledgments

We would like to thank the Indiana Center for Biological Microscopy, the IUSM Center for Electron Microscopy (iCEM), and the National Gene Vector Biorepository (NGVB). This work is funded by the NIH grants 1U54HL142019-01, 5R01HL130871-02, and 1P01HL160472-01.






References

- [1] M. C. Ozelo, J. Mahlangu, K. J. Pasi et al., "Valoctocogene roxaparvec gene therapy for hemophilia a," *New England Journal of Medicine*, vol. 386, no. 11, pp. 1013–1025, 2022.
- [2] Crossrates M, *AveXis receives FDA approval for Zolgensma®, the first and only gene therapy for pediatric patients with spinal muscular atrophy (SMA)*, Crossrates M, 2019.
- [3] D. A. Prado, M. Acosta-Acero, and R. S. Maldonado, "Gene therapy beyond luxturna: a new horizon of the treatment for inherited retinal disease," *Current Opinion in Ophthalmology*, vol. 31, no. 3, pp. 147–154, 2020.
- [4] M. F. Naso, B. Tomkowicz, W. L. Perry 3rd, and W. R. Strohl, "Adeno-associated virus (AAV) as a vector for gene therapy," *BioDrugs*, vol. 31, no. 4, pp. 317–334, 2017.
- [5] J. El Andari and D. Grimm, "Production, processing, and characterization of synthetic AAV gene therapy vectors," *Biotechnology Journal*, vol. 16, no. 1, 2021.
- [6] H. Zhao, W. H. Meisen, S. Wang, and K. J. Lee, "Process development of recombinant adeno-associated virus production platform results in high production yield and purity," *Human Gene Therapy*, vol. 34, no. 1-2, pp. 56–67, 2023.
- [7] M. Toueille, "Development of purification steps for several AAV serotypes using POROS™ CaptureSelect™ AAVX affinity chromatography," *Cell and Gene Therapy Insights*, vol. 2, no. 1, 2016.
- [8] S. G. Jacobson, G. M. Acland, G. D. Aguirre et al., "Safety of recombinant adeno-associated virus type 2-RPE65 vector delivered by ocular subretinal injection," *Molecular Therapy*, vol. 13, no. 6, pp. 1074–1084, 2006.
- [9] R. G. Weleber, M. E. Pennesi, D. J. Wilson et al., "Results at 2 years after gene therapy for RPE65-deficient Leber congenital amaurosis and severe early-childhood-onset retinal dystrophy," *Ophthalmology*, vol. 123, no. 7, pp. 1606–1620, 2016.
- [10] L. P. Lowes, L. N. Alfano, W. D. Arnold et al., "Impact of age and motor function in a phase 1/2A study of infants with SMA type 1 receiving single-dose gene replacement therapy," *Pediatric Neurology*, vol. 98, pp. 39–45, 2019.
- [11] K. D. Foust, X. Wang, V. L. McGovern et al., "Rescue of the spinal muscular atrophy phenotype in a mouse model by early postnatal delivery of SMN," *Nature Biotechnology*, vol. 28, no. 3, pp. 271–274, 2010.
- [12] G. A. Rodrigues, E. Shalaev, T. K. Karami, J. Cunningham, N. K. H. Slater, and H. M. Rivers, "Pharmaceutical development of AAV-based gene therapy products for the eye," *Pharmaceutical Research*, vol. 36, no. 2, p. 29, 2018.
- [13] Administration UFaD, *Chemistry, manufacturing, and control (CMC) information for human gene therapy investigational new drug applications (inds)*. 2020, Administration UFaD, 2021.
- [14] J. C. Grieger, S. M. Soltys, and R. J. Samulski, "Production of recombinant adeno-associated virus vectors using suspension HEK293 cells and continuous harvest of vector from the culture media for GMP FIX and FLT1 clinical vector," *Molecular Therapy*, vol. 24, no. 2, pp. 287–297, 2016.
- [15] J. F. Wright, "Product-related impurities in clinical-grade recombinant AAV vectors: characterization and risk assessment," *Biomedicines*, vol. 2, no. 1, pp. 80–97, 2014.
- [16] J. Zhang, M. Chrzanowski, D. A. Frabutt et al., "Cryptic resolution sites in the vector plasmid lead to the heterogeneities in the rAAV vectors," *Journal of Medical Virology*, vol. 95, no. 1, article e28433, 2023.
- [17] J. Zhang, P. Guo, X. Yu et al., "Subgenomic particles in rAAV vectors result from DNA lesion/break and non-homologous end joining of vector genomes," *Molecular Therapy-Nucleic Acids*, vol. 29, pp. 852–861, 2022.
- [18] D. Blessing, G. Vachey, C. Pythoud et al., "Scalable production of AAV vectors in orbitally shaken HEK293 cells," *Molecular Therapy - Methods & Clinical Development*, vol. 13, pp. 14–26, 2019.
- [19] Y. Pu, R. Katz, Y. Chen et al., "Development and application of a liquid chromatography-mass spectrometry method for residual Iodixanol quantification in AAV-based gene therapy product development," *Human Gene Therapy*, vol. 33, no. 1-2, pp. 103–108, 2022.
- [20] F. Mingozzi, X. M. Anguela, G. Pavani et al., "Overcoming preexisting humoral immunity to AAV using capsid decoys," *Science Translational Medicine*, vol. 5, no. 194, 2013.
- [21] J. F. Wright, "Codon modification and PAMPs in clinical AAV vectors: the tortoise or the hare?," *Molecular Therapy*, vol. 28, no. 3, pp. 701–703, 2020.
- [22] M. Hösel, M. Broxtermann, H. Janicki et al., "Toll-like receptor 2-mediated innate immune response in human nonparenchymal liver cells toward adeno-associated viral vectors," *Hepatology*, vol. 55, no. 1, pp. 287–297, 2012.
- [23] F. Mingozzi, M. V. Maus, D. J. Hui et al., "CD8(+) T-cell responses to adeno-associated virus capsid in humans," *Nature Medicine*, vol. 13, no. 4, pp. 419–422, 2007.
- [24] N. Paulk, "Gene therapy: it is time to talk about High-dose AAV," *Genetic Engineering & Biotechnology News*, vol. 40, no. 9, pp. 14–16, 2020.
- [25] (FDA) UFaDA, *Toxicity risks of adeno-associated virus (AAV) vectors for gene therapy (GT)*, Cellular, Tissue, and Gene Therapies Advisory Committee (CTGTAC) Meeting #70, 2021.

- [26] P. Gagnon, B. Goricar, N. Mencin et al., "Multiple-monitor HPLC assays for rapid process development, in-process monitoring, and validation of AAV production and purification," *Pharmaceutics*, vol. 13, no. 1, p. 113, 2021.
- [27] R. Dickerson, C. Argento, J. Pieracci, and M. Bakhshayeshi, "Separating empty and full recombinant adeno-associated virus particles using isocratic anion exchange chromatography," *Biotechnology Journal*, vol. 16, no. 1, article e2000015, 2021.
- [28] A. L. Hejmowski, K. Boenning, J. Huato, A. Kavara, and M. Schofield, "Novel anion exchange membrane chromatography method for the separation of empty and full adeno-associated virus," *Biotechnology Journal*, vol. 17, no. 2, article e2100219, 2022.
- [29] A. K. Lam, J. Zhang, D. Frabutt et al., "Fast and high-throughput LC-MS characterization, and peptide mapping of engineered AAV capsids using LC-MS/MS," *Molecular Therapy - Methods & Clinical Development*, vol. 27, pp. 185–194, 2022.
- [30] O. Cao, B. E. Hoffman, B. Moghimi et al., "Impact of the underlying mutation and the route of vector administration on immune responses to factor IX in gene therapy for hemophilia B," *Molecular Therapy*, vol. 17, no. 10, pp. 1733–1742, 2009.
- [31] J. M. Finlon, M. A. Burchill, and B. A. J. Tamburini, "Digestion of the murine liver for a flow cytometric analysis of lymphatic endothelial cells," *Journal of Visualized Experiments*, vol. 143, no. 143, article e58621, 2019.
- [32] S.-H. Kung, J. Nathan Hagstrom, D. Cass et al., "Human factor IX corrects the bleeding diathesis of mice with hemophilia B," *Blood, The Journal of the American Society of Hematology*, vol. 91, no. 3, pp. 784–790, 1998.

Research Article

Intra-Articular AAV9 α -L-Iduronidase Gene Replacement in the Canine Model of Mucopolysaccharidosis Type I

Raymond Yu-Jeang Wang ^{1,2}, Shih-Hsin Kan ³, Haoyue Zhang,⁴ Jodi D. Smith ⁵,
Afshin Aminian,⁶ Elizabeth Snella ^{7,8}, Jackie K. Jens,^{7,9} Sarah P. Young,^{4,10}
Patricia I. Dickson,¹¹ and N. Matthew Ellinwood ⁷

¹Division of Metabolic Disorders, CHOC Children's Specialists, Orange 92868, USA

²Department of Pediatrics, University of California-Irvine School of Medicine, Orange 92868, USA

³CHOC Children's Research Institute, Orange 92868, USA

⁴Biochemical Genetics Laboratory, Duke University Health System, Durham 27710, USA

⁵Department of Veterinary Pathology, Iowa State University, Ames 50011, USA

⁶Orthopedic Institute, CHOC Children's Hospital, Orange 92868, USA

⁷Department of Animal Science, Iowa State University, Ames 50011, USA

⁸Department of Genetics, Development, And Cell Biology, Iowa State University, Ames 50011, USA

⁹Department of Veterinary Clinical Sciences, Iowa State University, Ames 50011, USA

¹⁰Department of Pediatrics, Duke University, Durham 27710, USA

¹¹Division of Genetics and Genomic Medicine, Department of Pediatrics, Washington University School of Medicine in St. Louis, St. Louis 63130, USA

Correspondence should be addressed to Raymond Yu-Jeang Wang; rawang@choc.org

Received 4 February 2023; Revised 18 July 2023; Accepted 24 August 2023; Published 14 September 2023

Academic Editor: Dao Pan

Copyright © 2023 Raymond Yu-Jeang Wang et al. This is an open access article distributed under the Creative Commons Attribution License, which permits unrestricted use, distribution, and reproduction in any medium, provided the original work is properly cited.

Mucopolysaccharidosis type I (MPS I), an inherited lysosomal storage disorder characterized by deficiency of α -L-iduronidase (IDUA) activity, causes multisystemic pathology due to sequelae of accumulated heparan and dermatan sulfates (HS and DS), the substrates of IDUA. Current treatments, though life-prolonging, inadequately address skeletal dysplasia and do not forestall progressive and painful degenerative joint disease. Previous studies demonstrated that intra-articular enzyme replacement cleared cellular lysosomal storage and reduced joint inflammation. Three nontolerized MPS I canines were studied to assess safety, efficacy, and durability of IDUA gene replacement therapy delivered via intra-articular injection. After baseline joint tissue biopsies, the right shoulder and stifle of each animal were injected in the intra-articular space with AAV9-IDUA and contralateral joints with AAV9-eGFP. Animals received either 5E11 or 5E12 vector genomes/joint. Necropsy was performed at 2- or 52-week postinjection. All animals tolerated injections without adverse effects. At two weeks, supraphysiologic IDUA enzyme activity was measured in AAV9-IDUA-treated but not AAV9-eGFP-treated synovium, with corresponding normalization of HS content and synoviocyte morphology. The AAV9-IDUA-treated cartilage had normal physiologic levels of IDUA enzyme, reduced but not normalized HS and DS levels compared to untreated MPS I cartilage, and healthy chondrocyte morphology. Liver IDUA transgene and IDUA enzyme activity were identified, as was serum IDUA activity which was 40% of wild-type serum enzyme activity. At 52-week postinjection, AAV9-IDUA-treated synovium and cartilage IDUA enzyme activity declined in both animals, corresponding to high tissue HS and DS levels and severe lysosomal storage. Liver and serum IDUA activity levels were undetectable. A dose-dependent serum anti-IDUA antibody response was observed which, together with loss of transgene with age, likely contributed to decline in tissue enzyme activity and treatment efficacy. Our study demonstrates successful proof-of-concept for intra-articular gene replacement therapy as a treatment for MPS-related joint dysplasia. Our observations suggest the possibility of multimodal gene replacement therapy to address multiple refractory manifestations of MPS I. Subsequent studies, in conjunction with immune tolerization and functional assessments of joint pathology, will investigate this possibility.

1. Introduction

The mucopolysaccharidoses (MPSs) are a group of twelve inborn errors of metabolism caused by deficiency of glycosaminoglycan- (GAG-) degrading enzymes with resultant GAG storage in lysosomes and tissues and progressive multisystemic dysfunction [1, 2]. Mucopolysaccharidosis type I (MPS I), often referred to by the eponyms Hurler, Hurler-Scheie, and Scheie syndromes depending upon degree of central nervous system (CNS) involvement and velocity of disease progression, results from a deficiency of the activity of α -L-iduronidase (IDUA) and results in tissue storage of the GAG species heparan sulfate (HS) and dermatan sulfate (DS). Across the MPS I disease spectrum, affected individuals experience varying degrees of upper airway obstruction, cardiac valve dysplasia, hepatosplenomegaly, skeletal dysplasia, and neurologic involvement [3].

The storage of GAG in chondrocytes triggers an abnormal proliferation in epiphyseal cartilage and disturbed cartilage matrix, with subsequent skeletal dysplasia manifesting as abnormally shaped vertebral bodies (kyphosis), shallow acetabulae, hip dysplasia, and genu valgum [4]. Joint synovium is also affected, becoming hypertrophic and inflamed. Clinically, these changes result in painful degenerative joint disease, which severely reduces mobility, independence, and quality of life [5].

Treatments for MPS I, either hematopoietic stem cell transplant (HSCT) or intravenous enzyme replacement therapy (ERT) with recombinant human IDUA (rhIDUA), have reduced disease burden and extended life expectancy of MPS I patients into adulthood [6, 7]. The unifying premise of each therapy is the provision of functional IDUA enzyme to affected IDUA-deficient tissue, degrading accumulated HS and DS [8]. Clearance of accumulated substrate improves cellular function and ideally prevents subsequent symptomatology.

However, both HSCT and ERT are imperfect treatments. Undergoing HSCT entails significant risks of immunocompromise, graft-versus-host disease, incomplete engraftment, and/or death. Pursuit of ERT entails weekly IV infusions for the patient's entire lifetime and does not cross the blood-brain barrier (BBB) to any significant degree, thus rendering it incapable of treating the CNS disease of neuro-pathic MPS I. Neither HSCT nor ERT adequately treat orthopedic disease, ostensibly the consequence of negligible IDUA delivery and the continued GAG accumulation and pathology progression in joint tissues and chondrocytes [9, 10]. Treated MPS I patients suffer pain, immobility, and severely reduced quality of life due to progressive joint contractures, deformities, and arthritis [11, 12]. Surgical interventions are required to ameliorate these complications; due to their multisystem comorbid conditions, MPS I patients suffer increased perioperative morbidity and mortality [13]. Consequently, gene replacement therapy is an attractive option, as it is potentially a single-dose therapeutic providing long-term, durable transgene expression [14, 15].

In the canine model of MPS I, which recapitulates many aspects of human MPS I disease, we demonstrated that monthly intra-articular injections of rhIDUA were well tol-

erated and resulted in significant reduction of synoviocyte and chondrocyte lysosomal storage, with concomitant reduction of joint inflammatory macrophages [16]. However, repeated articular injection into multiple affected joints is not ideal for MPS I patients. Herein, we report on the safety and efficacy results of a proof-of-concept study utilizing adeno-associated virus (AAV) serotype 9-mediated canine *IDUA* (*cIDUA*; hereafter referred to as *IDUA*) gene replacement, delivered intra-articularly to the MPS I canine model system.

2. Materials and Methods

2.1. IACUC. This study was conducted under compliance approvals obtained from the Iowa State University IACUC (protocols 12-04-5791-K and 2-18-8714-K) and Institutional Biosafety Committee (protocol 18-D-0004-A). All dogs used in the study were bred and maintained at Iowa State University in accordance with the USDA and NIH guidelines for the care of dogs. The MPS I dog colony was maintained on a mixed genetic background. Animals were housed together for enrichment and provided enrichment items. Their environment was set to have constant 72-degree F temperature, humidity, 12-hour/12-hour light: dark cycles, and air circulated 15 times an hour. Animals had continuous access to water and were fed *ad libitum*. Breedings were conducted by artificial insemination, crossing heterozygous females and heterozygous or MPS I-affected males. MPS I-affected animals were identified by IDUA enzymatic assay and polymerase chain reaction in whole blood [17].

2.2. Vector Prep. The AAV9 vector contains a payload consisting of the chicken β -actin promoter, the cytomegalovirus immediate early enhancer, a codon-optimized *IDUA* or *eGFP* sequence, and the rabbit β -globin polyadenylation sequence. Vector was produced by triple transfection of HEK293T cells, purified on iodixanol gradients, and assessed for infectious capacity and endotoxin content as described by Wang, et al. [18].

2.3. Treatment. All animals received only intra-articular AAV vector and did not receive predose tolerization. Four weeks (see Safety) after baseline synovial and cartilage biopsies, one animal (low-dose +52 w) received 5E11 vg/joint AAV9-*IDUA* into the right shoulder and stifle and was necropsied 52-week postdosing. Four weeks following baseline biopsies, two animals received 5E12 vg/joint AAV9-*IDUA* into the right shoulders and stifles; one was euthanized 2 weeks following treatment (high-dose +2 w) and the other 52 weeks following treatment (high-dose +52 w). All three animals' contralateral shoulder and stifle joints were injected with AAV9-green fluorescent protein (eGFP) at doses corresponding to their AAV9-*IDUA* dose. Please refer to Figure 1 for a schematic of the study. Following injection, monthly complete blood counts with differential, electrolytes, transaminases, blood urea nitrogen, creatinine, bilirubin, albumin, and protein were obtained.

2.4. Necropsy. All three AAV-treated dogs were euthanized with intravenous sodium pentobarbital overdose

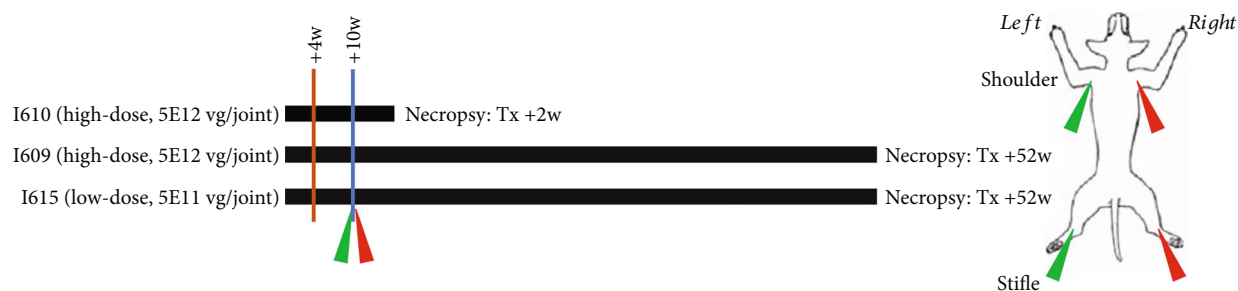


FIGURE 1: Study schematic. Four weeks after birth and six weeks prior to treatment, the three animals underwent pretreatment biopsy (brown vertical line). Treatment (blue vertical line) took place ten weeks after birth with dosages, vectors, and injection sites as designated. Necropsy took place +2 weeks after treatment (I610) or +52 weeks after treatment (I609 and I615). Green arrow indicates treatment with AAV9-*eGFP*; red arrow indicates treatment with AAV9-*IDUA*.

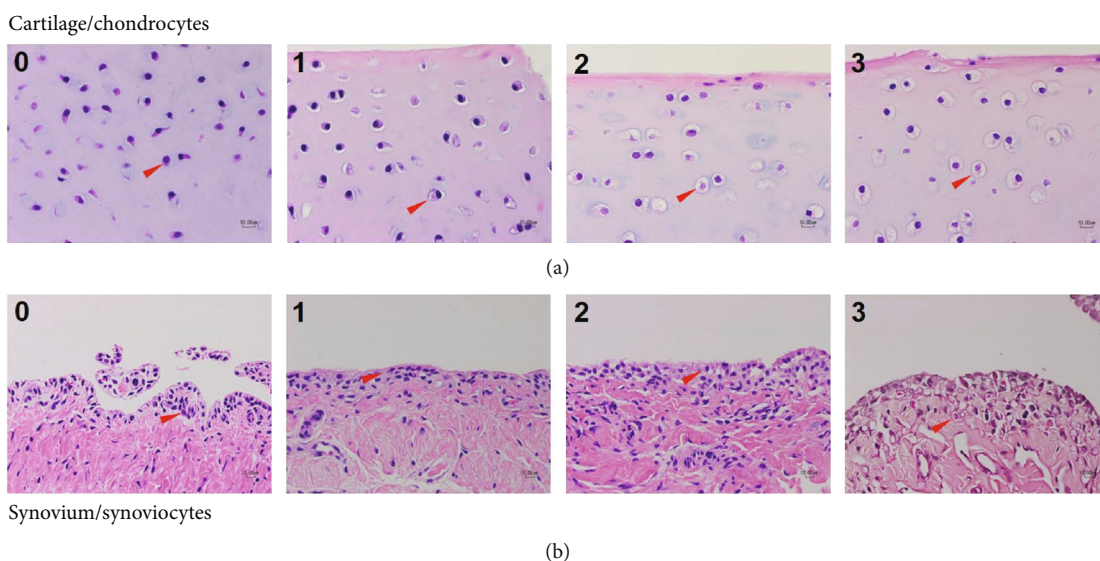


FIGURE 2: Exemplary joint tissue photomicrographs. Cartilage (a) and synovium (b) photomicrographs demonstrate scoring schema for lysosomal storage in chondrocytes and synoviocytes, respectively. Representative cells are denoted by red arrowheads.

TABLE 1: Absolute (% of wild-type) serum IDUA enzyme activity of the three animals treated in this study with respect to timing of treatment.

	Time of necropsy	Time pre-/post-intra-articular AAV9 treatment					
		-6 w	+2 w	+12 w	+24 w	+18 w	+52 w
High-dose 5E12 vg/joint	+2 w	0.00 (0%)	2.16 (49.5%)				
High-dose 5E12 vg/joint	+52 w	0.00 (0%)	n.m.	0.07 (1.6%)	0.11 (2.5%)	0.14 (3.2%)	0.00 (0%)
Low-dose 5E11 vg/joint	+52 w	0.00 (0%)	n.m.	0.00 (0%)	0.02 (0.46%)	0.05 (1.1%)	0.00 (0%)

All animals have undetectable serum enzyme at baseline (6 weeks prior to treatment); enzyme activities approach 50% of normal two weeks following treatment but decline afterwards, eventually returning to baseline at 52 weeks. Wild-type animal serum IDUA enzyme is 4.36 ± 1.31 units/mL. Data were generated from at least three independent experiments and shown as mean \pm SD. n.m.: not measured.

at either 2- or 52-week posttreatment. All dogs were necropsied immediately following euthanasia. Aspiration of the shoulder and stifle joints was attempted for synovial fluid collection. Cartilage and synovium samples were collected from the proximal and distal surfaces of bilateral glenohumeral/shoulder and tibiofemoral/stifle joints. Samples were collected into 4% paraformaldehyde or flash frozen in liquid nitrogen. After 24 hours of fixation, samples for histology were processed by routine methods and embedded

in paraffin. Serial $5 \mu\text{m}$ thick sections were cut for histochemical staining. Tissues were obtained from three age-matched wild-type and three untreated MPS I-affected animals to be used as controls for biochemical assays and histology.

2.5. Histopathology and Scoring. Histologic sections were deparaffinized in xylene and rehydrated through graded concentrations of ethanol. Sections were stained in

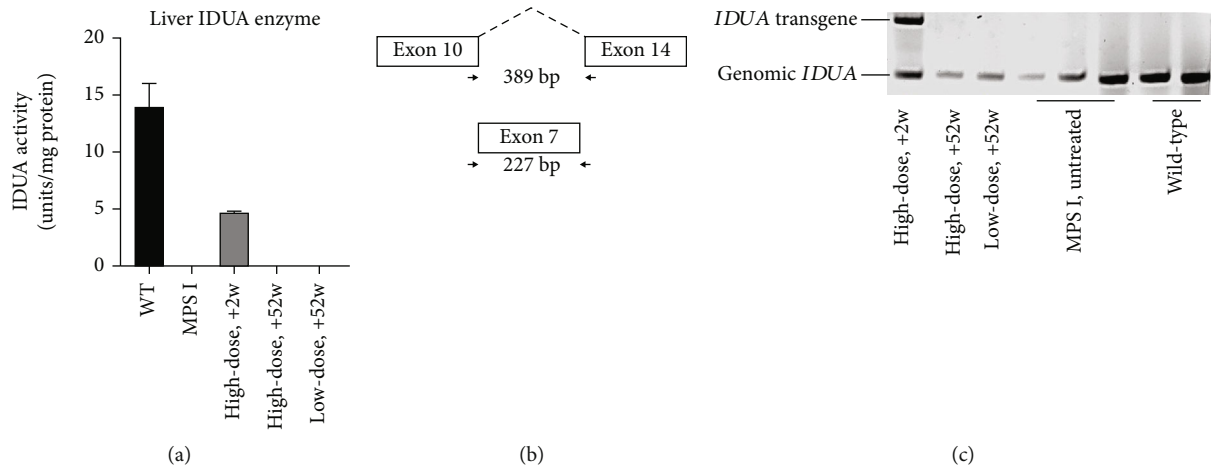


FIGURE 3: (a) IDUA enzyme activity measurements from homogenates from wild-type, MPS-I untreated, and study animals. Data were generated from at least three independent experiments and shown as mean \pm SD. (b) Schematic of PCR primers utilized to detect the *IDUA* transgene (389 base pairs spanning cDNA between exon 10 and exon 14) and the native genomic *IDUA* gene (227 bp covering the entirety of exon 7). (c) Transgene and genomic *IDUA* PCR of liver homogenates. The presence of the native *IDUA* gene is identified in all animals, but only the high-dose +2 w dog demonstrates the presence of *IDUA* transgene and appreciable levels of IDUA enzyme in liver. The two +52 w animals had neither measurable liver IDUA enzyme activity nor *IDUA* transgene.

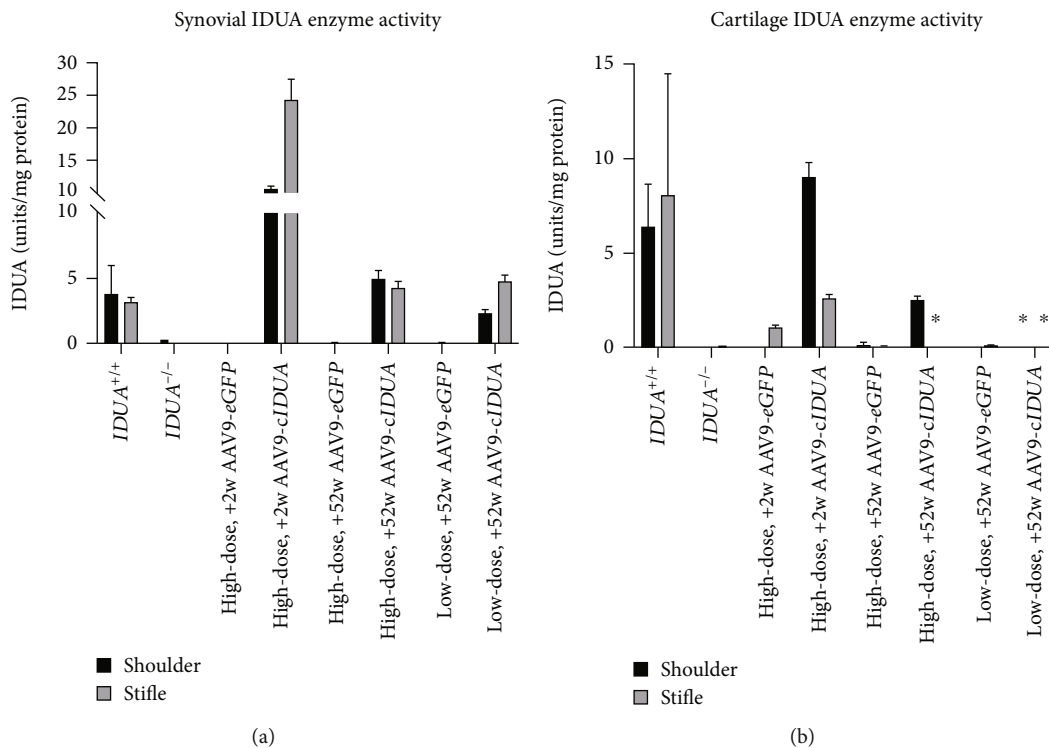


FIGURE 4: Joint tissue IDUA enzyme activity measurements. At 2 weeks, supraphysiologic enzyme levels are synthesized in AAV9-*IDUA*-treated synovium (a) (note y-axis) and physiologic levels in cartilage (b). AAV9-eGFP-treated tissues demonstrate undetectable to trace levels of IDUA enzyme. Synovial and cartilage IDUA levels are present in 52-week AAV9-*IDUA*-treated tissues. Data were generated from at least three independent experiments and shown as mean \pm SD. * could not be assayed.

hematoxylin and eosin (H&E), dehydrated, cleared, and mounted. All sections were prepared and examined by the same pathologist, who was blinded to animal identity and treatment status, using a Nikon Eclipse Ci brightfield microscope and photomicrographs acquired with a Nikon DS-Fi2 color CCD camera.

Lysosomal distension of synoviocytes and chondrocytes was scored on a scale of 0–3 as follows: 0 signifies little to no storage (cytoplasm is devoid of vesicles); 1 signifies mild storage (cytoplasm with small number of vesicles); 2 signifies moderate storage (cell is predominantly vesicles with a small amount of cytoplasm); and 3 signifies severe (cell is entirely

TABLE 2: Comparison of baseline and postnecropsy synovial HS and DS levels in intra-articular AAV9-treated-MPS I canines.

	Baseline	Necropsy	Percent change
<i>Heparan sulfate</i>			
Synovial HS high-dose +2 w			
AAV9- <i>eGFP</i> shoulder	1.87	1.64	-12.3%
AAV9- <i>eGFP</i> stifle	3.01	3.78	25.6%
AAV9- <i>IDUA</i> shoulder	1.95	0.14	-92.8%
AAV9- <i>IDUA</i> stifle	4.11	0.04	-99.0%
Synovial HS high-dose +52 w			
AAV9- <i>eGFP</i> shoulder	0.83	5.14	519%
AAV9- <i>eGFP</i> stifle	4.5	19.4	331%
AAV9- <i>IDUA</i> shoulder	1.73	1.63	-5.8%
AAV9- <i>IDUA</i> stifle	2.79	1.25	-55.2%
Synovial HS low-dose +52 w			
AAV9- <i>eGFP</i> shoulder	1.27	4.35	243%
AAV9- <i>eGFP</i> stifle	1.17	9.59	720%
AAV9- <i>IDUA</i> shoulder	0.22	2.87	1205%
AAV9- <i>IDUA</i> stifle	2.16	3.17	46.8%
<i>Dermatan sulfate</i>			
Synovial DS high-dose +2 w			
AAV9- <i>eGFP</i> shoulder	6.64	4.1	-38.3%
AAV9- <i>eGFP</i> stifle	12.32	5.78	-53.1%
AAV9- <i>IDUA</i> shoulder	8.64	1.84	-78.7%
AAV9- <i>IDUA</i> stifle	12.5	0.8	-93.6%
Synovial DS high-dose +52 w			
AAV9- <i>eGFP</i> shoulder	3.52	9.72	176%
AAV9- <i>eGFP</i> stifle	10.13	13.1	29.3%
AAV9- <i>IDUA</i> shoulder	1.87	4.23	126%
AAV9- <i>IDUA</i> stifle	7.19	2.56	-64.4%
Synovial DS low-dose +52 w			
AAV9- <i>eGFP</i> shoulder	3.46	12.69	267%
AAV9- <i>eGFP</i> stifle	4.98	8.68	74.3%
AAV9- <i>IDUA</i> shoulder	0.43	4.55	958%
AAV9- <i>IDUA</i> stifle	4.33	3.81	-12.0%

lysosomal vesicles) storage. Photomicrographs examples of synoviocytes and chondrocytes corresponding to each storage score are provided in Figure 2.

2.6. Enzymology. For biochemical assays, canine tissues were homogenized in CellLytic M cell lysis reagent (Millipore-Sigma). Iduronidase activity was assessed using 10 μ L of tissue homogenate or serum incubated with 4-methylumbelliferyl α -L-iduronide substrate (4-MUI) (Biosynth) at the final concentration of 0.25 mM for 1 hr at 37°C in a 96-well plate. Reactions were quenched with 180 μ L glycine carbonate buffer, and pH 10.5 and fluorescence measurements were obtained using an Infinite M Plex spectrofluorometer (Tecan) at excitation and emission

wavelengths of 360 nm and 450 nm, respectively. One activity unit was defined as 1 nmol of 4-methylumbelliferone released per hour. Protein concentration was estimated using the Pierce BCA assay kit (ThermoFisher), and bovine serum albumin provided from the kit was served as a standard. Measurements were made blinded to identity of the animal and treatment administered, in triplicate, and reported as specific activity (units of activity per mg of protein) for tissue samples and units/mL for serum samples.

2.7. Tissue PCR Amplification. Total genomic DNA was extracted from tissue homogenate by the Genomic DNA Clean and Concentrator (Zymo Research, Irvine, CA). The DNA samples were amplified with two sets of PCR primer pairs with the following sequences: *IDUA* F3 (5'-AGTTCCGGCGCATGCGCGCAGC-3'); *IDUA* R3 (5'-CGGTCCGGCCAGTAGTCCACC-3'); *IDUA* F4 (5'-GTGGTGCTGAGGTCAGTCTCCG-3'); *IDUA* R4 (5'-CGGGCA GGGCCTGGGGTCTCTAC-3'). The F3 and R3 primers are located within *IDUA* exon 10 and exon 14, respectively, and will amplify only transgenic *IDUA* cDNA sequences with an expected amplicon size of 389 bp; the F4 and R4 *IDUA* primers are located within *IDUA* intron 6 and intron 7, respectively, which amplify the endogenous *IDUA* gene with an expected amplicon size of 227 bp.

2.8. Glycosaminoglycan Quantification. Lyophilized tissue extract was desalted using Amicon 3k columns (Millipore) and eluted with diH₂O to the final concentration of 0.1 mg/ μ L (tissue dry weight/H₂O volume) before HS and DS analyses. Twenty-five μ L of tissue extracts, calibrators, and QC samples were transferred to a 12 \times 32 mm maximum recovery vials (Waters Corporation, Milford, MA) and evaporated under nitrogen at 35°C. The samples were mixed with 200 μ L of 3 M HCl in MeOH, incubated at 65°C for 65 min, and evaporated under nitrogen at ambient temperature. The samples were reconstituted in 25 μ L of internal standard solution and 200 μ L of matrix (10 mM NH₄OAc) in acetonitrile: H₂O (90:10, v : v). The samples were injected on an Acquity UPLC® I-class system coupled with a Xevo TQ-S micro mass spectrometer (Waters Corporation) with electron spray ionization in positive ion mode. Methylated HS and DS dimers and the corresponding deuteriomethylated HS and DS dimers were separated on a UPLC® BEH Amide 1.7 μ m, 2.1 \times 50 mm column (Waters Corp.) using a linear gradient as previously described [19]. Data were acquired by selected reaction monitoring (SRM) using the protonated molecular ion transition m/z 426 \rightarrow 236 for DS dimers, m/z 432 \rightarrow 239 for ²H6-DS dimers, the sodiated molecular ion transition m/z 406 \rightarrow 245 for HS dimers, and m/z 412 \rightarrow 251 for ²H6-HS dimers. Calibration curves were constructed using linear regression of responses (peak area ratios of HS and DS dimers to the corresponding deuterium-labeled dimers) to the concentrations of calibrators using TargetLynx® software (Waters Corp.) with 1/x weighting. Assessors were blinded to tissue type, genotype/treatment status of animal, and treatment administered.

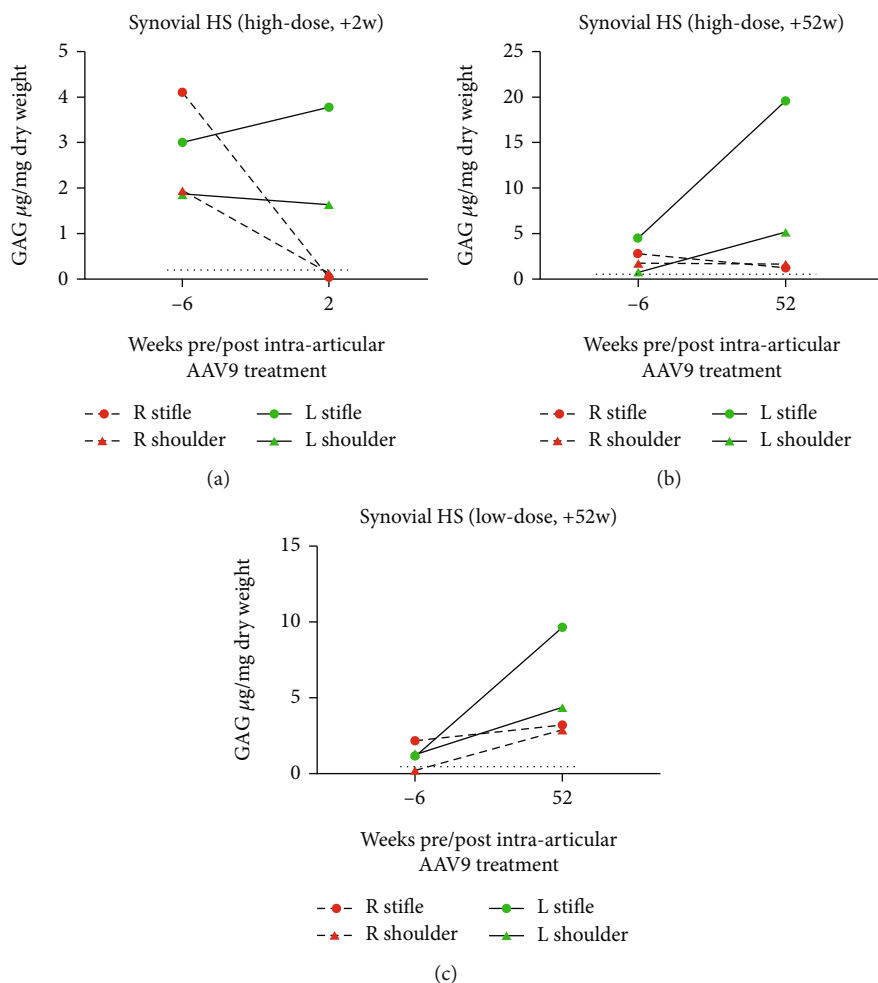


FIGURE 5: Synovial HS levels in the (a) high-dose +2 w, (b) high-dose +52 w, and (c) low-dose +52 w animals. Levels of synovial HS GAG at baseline (-6 weeks prior to AAV9 treatment) compared to levels at necropsy (+2- or +52-week post-AAV9 treatment). AAV9-IDUA joints are denoted in green, while AAV9-eGFP joints are denoted in red. The black dotted lines refer to synovial HS levels in age-matched normal dogs.

2.9. Anti-rhIDUA Serology. Serum and synovial fluid IgG antibodies against IDUA were measured by ELISA. Briefly, 96-well plates (Immulon 1B U-bottom microtiter plates, Corning, Corning, NY) were coated overnight with $0.2 \mu\text{g}$ IDUA in PBS. Following blocking with 3% BSA, serial diluted serum samples were added in triplicate to IDUA-coated wells and incubated at 37°C for 1 hr. The plates were washed, and specific binding of serum anti-IDUA antibodies to the coated wells was detected using alkaline-phosphatase-conjugated goat anti-dog IgG secondary antibody (Southern Biotechnology, Birmingham, AL). Absorbance values at 405 nm were measured as optical density (OD) using an Infinite M Plex spectrofluorophotometer (Tecan) after 1 mg/mL p-nitrophenol phosphate substrate (Sigma-Aldrich, St. Louis, MO) was added and developed at room temperature. The antibody titer is defined as the highest dilution of each sample with OD value higher than the background control. The OD value for a sample was taken from dilutions within the linear signal range.

2.10. Statistical Methods. Due to semiannual animal estrus, low litter size, and 25% rate of inheriting MPS I, no power calculation was performed. All animals identified to have MPS I were utilized for this study; an equal number (three) of treated MPS I, untreated MPS I, and wild-type animals were utilized. Results are reported as mean \pm SD and as -fold of wild-type levels. Postnecropsy HS and DS levels are reported as quantitative values and as a percentage of baseline HS and DS levels, respectively.

3. Results

3.1. Safety. All three animals tolerated anesthesia, baseline tissue biopsies, and AAV9 joint injections well, ambulating within 12 hours of surgery without discomfort or lameness. The low-dose +52 w animal experienced a right hock hygroma and joint effusion following tissue biopsy. The excess fluid was drained via needle puncture, and the joint capsule was allowed to heal completely, delaying vector

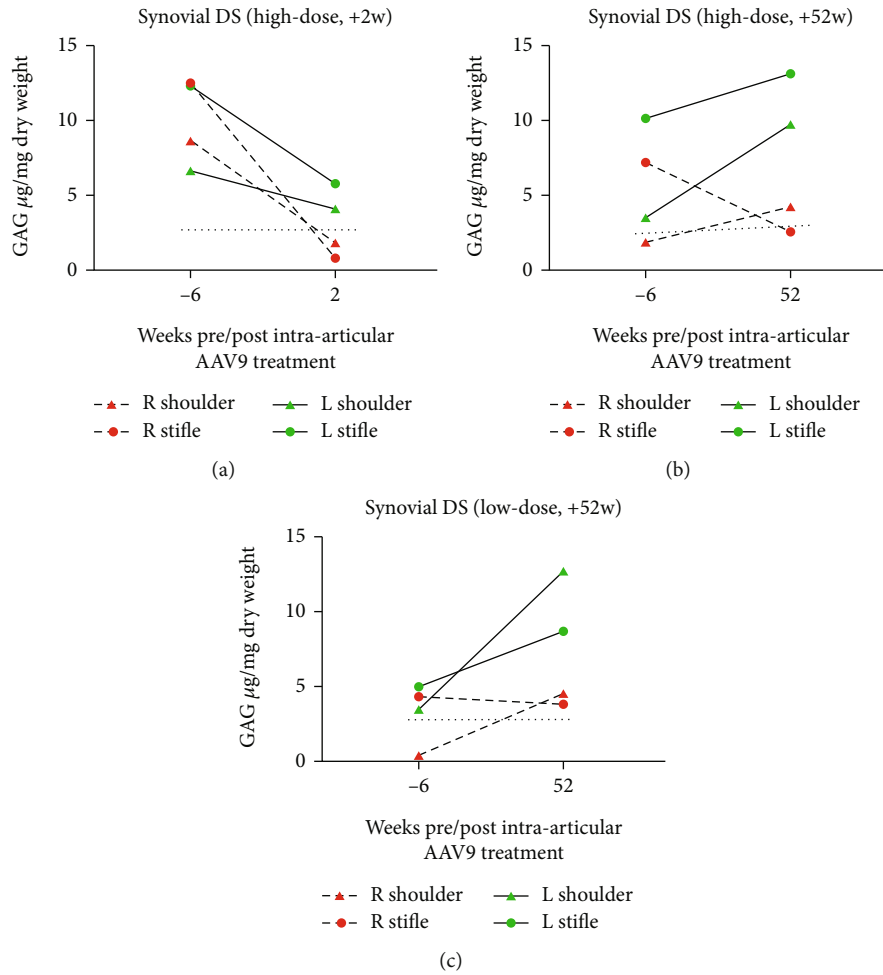


FIGURE 6: Synovial DS levels in the (a) high-dose +2 w, (b) high-dose +52 w, and (c) low-dose +52 w animals. Levels of synovial DS GAG at baseline compared to levels at necropsy. AAV9-IDUA joints in all three animals demonstrate synovial DS reduction, while AAV9-eGFP-treated joints show increases in DS levels in the two +52 w animals. The etiology for the DS reduction in AAV9-eGFP-treated joints in the +2 w-treated animal is unclear as its synovium has no measurable IDUA enzyme.

injection by two weeks (six-week postbiopsy). For consistency, the other two animals were also treated with vector at six-week postbiopsy (Figure 1). None of the animals experienced clinically significant abnormalities in hematology or serum chemistries throughout the study. Only the high-dose +2 w animal yielded synovial fluid in the shoulder and stifle joints at baseline and necropsy; no inflammatory cells were noted at baseline. At necropsy, synovial fluid in all joints demonstrated evidence of mild to moderate inflammation (neutrophils and activated macrophages).

3.2. Efficacy

3.2.1. *Clinical Assessments.* At the time of necropsy, both low-dose +52 w and high-dose +52 w animals displayed facial dysmorphism and joint laxity characteristic of canines with MPS I.

3.2.2. *Serum and Liver Treatment Effects.* At necropsy, the high-dose +2 w animal had serum IDUA enzyme activity

measured at 2.16 ± 0.27 units/mL, which was 49.5% of mean wild-type serum IDUA (4.36 ± 1.31 units/mL). Unfortunately, we do not have corresponding serum blood draws for either the low-dose +52 w or high-dose +52 w animals at the same time point (two-week posttreatment). Serum enzyme activity levels in these two animals were measurable but quite low in both animals at 8-, 13-, and 22-week post-treatment but declined to zero by the time of necropsy (see Table 1).

The liver of the high-dose +2 w dog had IDUA enzyme activity measured at 1.60 ± 0.11 units/mg protein, which was 34.8% of wild-type liver homogenate) and the presence of the IDUA transgene was evident by PCR. These findings suggest that the probable source of serum IDUA enzyme was the liver and not from leakage of IDUA enzyme from transduced joint tissues into the circulation. The low-dose +52 w and the high-dose +52 w animals demonstrated minimal IDUA enzyme activity and undetectable transgene in liver homogenates, indicating that transgene and expression declined significantly over time (see Figure 3). However,

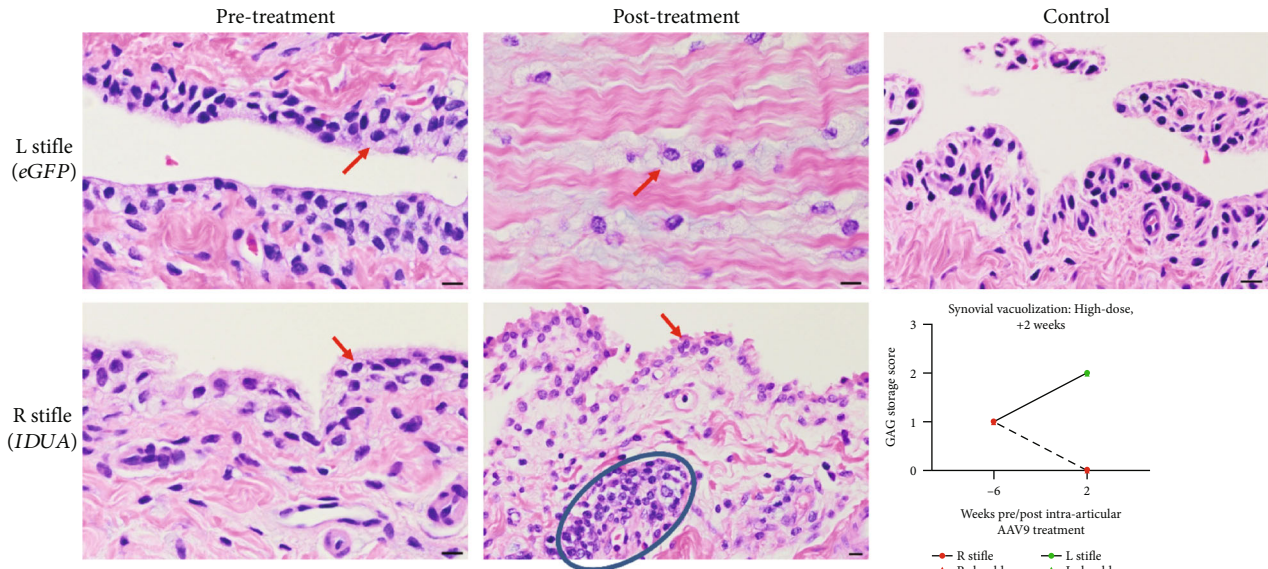


FIGURE 7: Synovial photomicrographs and lysosomal storage scoring in the high-dose +2 w animal. Baseline synoviocytes demonstrate lysosomal storage (red arrows, scored 1). At necropsy, AAV9-*eGFP* treated joint capsule showed increased lysosomal storage (scored 2), while AAV9-*IDUA*-treated synoviocytes scored 0. The latter also demonstrated a lymphocytic infiltrate (blue ellipse). Control synovium included for comparison. Bar = 10 μ M.

these findings raise the possibility that the liver can serve as an “*IDUA* depot,” synthesizing enzyme for other body tissues.

3.2.3. Synovium Treatment Effects

(1) *IDUA* Expression and Enzyme Activity. The AAV9-*IDUA*-treated joints of the high-dose +2 w animal had synovial *IDUA* enzyme activity levels which were 2.97–6.91 fold that of wild-type dog synovium (3.50 ± 1.59 units/mg protein). Only the right shoulder synovium of this animal (*IDUA* activity, 10.44 ± 0.59 units/mg protein) had detectable *IDUA* transgene, while the right stifle synovium (*IDUA* activity, 24.20 ± 3.35 units/mg protein) had no measurable *IDUA* transgene signal (see Figure 1S). The high-dose +52 w (shoulder: 4.97 ± 0.66 units/mg protein, 1.42-fold wild-type; stifle: 4.23 ± 0.56 units/mg protein, 1.2-fold wild-type) and low-dose +52 w (shoulder: 2.27 ± 0.34 units/mg protein, 0.65-fold wild-type; stifle: 4.78 ± 0.49 units/mg protein, 1.36-fold wild-type) animals both had synovial *IDUA* enzyme activity in AAV9-*IDUA*-treated joints measured at levels comparable to wild-type dogs (see Figure 4). The *IDUA* transgene was not detected in any of the AAV9-*eGFP*-treated joints, which also had *IDUA* enzyme activity levels that were comparable to that of the synovium measured in untreated MPS I dogs.

(2) *Synovial GAG Quantitation*. The HS and DS levels measured in synovial tissue of AAV9-*IDUA*-treated joints were decreased relative to untreated joints. Please refer to Table 2 for depiction of the data in chart format. In all animals, only AAV9-*IDUA*-treated joints demonstrate HS reduction. The greatest effect is seen in the high-dose +2 w animal, whose synovial HS levels are comparable to wild-type synovium.

The high-dose +52 w treated animal demonstrated synovial HS at near-normal levels, while the low-dose +52 w animal demonstrated synovial HS above levels seen in wild-type and increased slightly from baseline. Meanwhile, all AAV9-*eGFP*-treated joints demonstrated higher HS levels than AAV9-*IDUA*-treated joints (see Figure 5).

The measured levels of DS were similar to that of HS. Only AAV9-*IDUA* joints demonstrate DS reduction. The greatest effect is seen in the high-dose +2 w animal, whose AAV9-*IDUA*-treated synovial DS levels are comparable to wild-type synovial DS levels. Both +52 w-treated animals showed AAV9-*IDUA* synovial DS levels that were comparable to, or slightly above, normal animals, while DS levels in the AAV9-*eGFP*-treated joints increased over time (see Figure 6).

(3) *Synovial Histopathology*. In the high-dose +2 w animal, histology examination of necropsy samples documented normal synoviocyte morphology with no visible synovial lysosomal storage (scored 0). Contralateral AAV9-*eGFP* treated tissue yielded joint capsule, not synovium. Capsular cells were documented to have abundant intracellular storage granules (scored 2). Lymphocytic infiltrates were noted only in AAV9-*IDUA*-treated synovium, not AAV9-*eGFP*-treated synovium (Figure 7). The scores of synovium from animals treated for 52 weeks were consistent with a dose-response, with the high-dose +52 w animal scoring 1 in AAV9-*IDUA* joints (*eGFP* joints scored 2) and low-dose +52 w animal scoring 3 in AAV9-*IDUA* joints (*eGFP* joints scored 3) (Figure 2S).

3.2.4. Cartilage Treatment Effects

(1) *IDUA* Enzyme Activity. The high-dose +2-week animal had cartilage *IDUA* enzyme activity levels which were

TABLE 3: Comparison of baseline and post-necropsy cartilage HS and DS levels in intra-articular AAV9-treated-MPS I canines.

	Baseline	Necropsy	Percent change
<i>Heparan sulfate</i>			
Cartilage HS high-dose +2 w			
AAV9- <i>eGFP</i> shoulder	0.7	0.75	7.1%
AAV9- <i>eGFP</i> stifle	0.25	0.49	96.0%
AAV9- <i>IDUA</i> shoulder	0.72	0.41	-43.1%
AAV9- <i>IDUA</i> stifle	0.66	0.31	-53.0%
Cartilage HS high-dose +52 w			
AAV9- <i>eGFP</i> shoulder	0.35	9.01	2474%
AAV9- <i>eGFP</i> stifle	0.79	12.7	1508%
AAV9- <i>IDUA</i> shoulder	1.68	5.4	221%
AAV9- <i>IDUA</i> stifle	0.9	8.96	896%
Cartilage HS low-dose +52 w			
AAV9- <i>eGFP</i> shoulder	0.42	7.09	1588%
AAV9- <i>eGFP</i> stifle	1.26	7.33	482%
AAV9- <i>IDUA</i> shoulder	0.99	5.99	505%
AAV9- <i>IDUA</i> stifle	1.04	8.82	748%
<i>Dermatan sulfate</i>			
Cartilage DS high-dose +2 w			
AAV9- <i>eGFP</i> shoulder	2.58	3.3	27.9%
AAV9- <i>eGFP</i> stifle	3.56	4.11	15.4%
AAV9- <i>IDUA</i> shoulder	0.4	2.43	508%
AAV9- <i>IDUA</i> stifle	3.66	4.05	10.7%
Cartilage DS high-dose +52 w			
AAV9- <i>eGFP</i> shoulder	0.27	15.69	5711%
AAV9- <i>eGFP</i> stifle	2.36	21.09	794%
AAV9- <i>IDUA</i> shoulder	3.41	14.22	317%
AAV9- <i>IDUA</i> stifle	3.46	14.14	309%
Cartilage DS low-dose +52 w			
AAV9- <i>eGFP</i> shoulder	0.29	15.22	5148%
AAV9- <i>eGFP</i> stifle	4.24	13.64	222%
AAV9- <i>IDUA</i> shoulder	0.44	12.33	2702%
AAV9- <i>IDUA</i> stifle	3.14	17.5	457%

0.36-1.25-fold that of wild-type cartilage (7.25 ± 4.61 units/mg protein). Specifically, right shoulder cartilage demonstrated IDUA activity of 9.03 ± 0.76 units/mg protein, and right stifle cartilage showed IDUA activity of 2.59 ± 0.21 units/mg protein. Cartilage IDUA enzyme activity was 2.52 ± 0.20 units/mg protein in the right shoulder of the high-dose +52-week animal (0.35-fold wild-type). With the exception of stifle cartilage in the high-dose +2w pup (15% of wild-type), only very low (<1.7% of wild-type) IDUA activity was detected in AAV9-*eGFP*-treated cartilage (see Figure 4).

(2) *Cartilage GAG Quantitation*. AAV9-*IDUA* resulted in treatment effects for both HS and DS in cartilage. Please refer to Table 3 for depiction of the data in chart format.

Only the AAV9-*IDUA*-treated joints of the high-dose +2w animal demonstrated reduction of cartilage HS, which was still higher than wild-type control cartilage HS. The AAV9-*IDUA*-treated cartilage of the high-dose +52w animal had lower HS levels relative to contralateral AAV9-*eGFP*-treated joints, but this level was still markedly above that of normal cartilage. The low-dose +52w animal had cartilage HS levels measured at the level of an affected joint (see Figure 8).

In all animals, cartilage DS increased from baseline to necropsy. The AAV9-*IDUA*-treated cartilage of the high-dose +2w animal had DS levels that were lower relative to the contralateral AAV9-*eGFP*-treated joints but that were still elevated above wild-type cartilage DS levels. Both the high-dose +52w and low-dose +52w animals' cartilage DS levels were increased relative to baseline (see Figure 9).

(3) *Chondrocyte Histopathology*. Only in the high-dose +2w animal was there a clearance of chondrocyte lysosomal storage from baseline (Figure 10). In the two +52w animals, all joint chondrocytes, regardless of treatment status, were documented to have severe vacuolization and lysosomal storage granules (Figure 3S).

3.2.5. *Immunologic Assays*. No animal had serum anti-IDUA antibodies present at baseline. The results of anti-IDUA antibody ELISA conducted on necropsy sera identified the highest anti-IDUA IgG titers in serum of the high-dose +52w animal (1:25,600 dilution). The low-dose +52w animal developed a low serum anti-IDUA titer (1:800 dilution), and the high-dose +2w animal had no measurable serum anti-IDUA antibodies, likely due to the short period of time between vector injection and necropsy (Figure 11). Synovial anti-IDUA antibodies were weakly positive (1:300) in all joints of the high-dose +2w animal. The only synovial fluid sample available in the +52w animals was the high-dose left (AAV9-*eGFP*) stifle with a moderately positive (1:2,700) titer.

4. Conclusion

Effective therapy for MPS-related arthropathy has been elusive; neither standard-of-care intravenous ERT nor HSCT deliver sufficient IDUA enzyme activity to joint synovium or cartilage for adequate tissue GAG clearance. Preclinical work in canine MPS I and VII have documented that supra-physiologic blood IDUA activity levels are required for therapeutic effect in difficult-to-treat areas such as cardiac valves and articular cartilage [20, 21]. Human MPS I clinical trial results corroborate this finding. Recent reports of treatment with autologous lentiviral-IDUA-transduced hematopoietic stem/progenitor cell transplant yielded blood IDUA activity levels 2.7- to 12.5-fold above median normal levels and gradual improvement in shoulder and knee joint range of motion 6-9 months posttransplant [22].

We aimed to assess whether intra-articular AAV *IDUA* gene replacement therapy could affect high-level joint IDUA expression, tissue GAG reduction, and ameliorate MPS I arthropathy. Intra-articular AAV-based therapies have been tested preclinically, primarily for osteoarthritis or rheumatoid

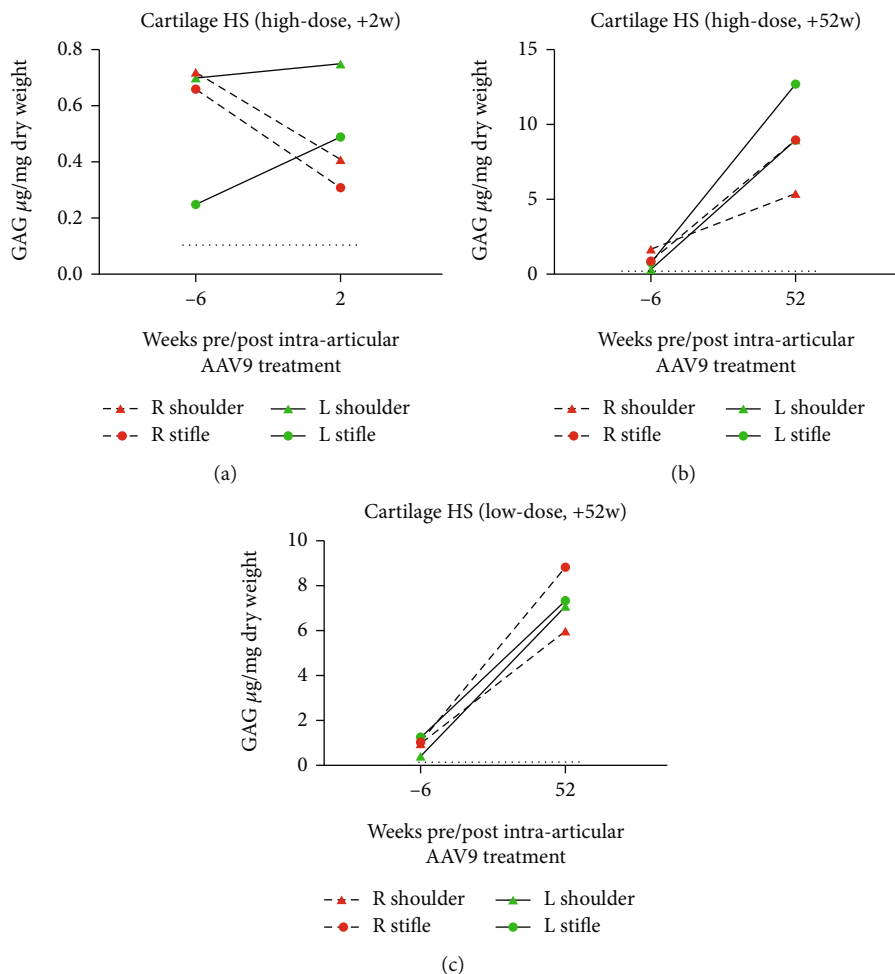


FIGURE 8: Cartilage HS levels in the (a) high-dose +2 w, (b) high-dose +52 w, and (c) low-dose +52 w animals. HS is only reduced in AAV9-IDUA-treated cartilage of the high-dose +2 w dog. In all other joints, cartilage HS was higher at necropsy than at baseline.

arthritis indications in small and large animal model systems; several are currently in human clinical trials. One intra-articular nonviral gene replacement therapy has been reported for MPS I mice, employing IDUA plasmid nanoemulsions which resulted in supraphysiologic synovial fluid IDUA enzyme levels 48 hours posttreatment [23]. As the nanoemulsion method only expressed enzyme for up to 7 days, intra-articular gene replacement using viral vectors, which for intravenous delivery results in longer-term transgene expression, represented a potentially more viable therapeutic approach for MPS I arthropathy.

Our study documents that AAV9-IDUA intra-articular injections at the 5E11 and 5E12 vg/joint dosages were safe and well tolerated in MPS I canines without adverse effects to clinical status, hematologic parameters, electrolytes, or transaminases. Two weeks following injection, we identified high levels of IDUA enzyme activity in necropsied synovium and more modest, but significantly elevated, IDUA activity levels in cartilage, serum, and liver. The IDUA activity levels correlated with degree of substrate clearance, with normalization of synovial HS and DS GAG and lysosomal histopathology scores; and reduction of cartilage HS and DS GAG,

and normal, basophilic chondrocyte morphology. Although IDUA enzyme has higher V_{max} and lower K_m for DS [24], HS appears to be a more sensitive marker to treatment response, as it is largely absent from normal synovium and cartilage. Though KS and DS storage are more classically associated with articular pathology in MPS, HS storage does appear to contribute to arthropathy too, as it has proinflammatory properties [25, 26]. MPS type III patients also have some degree of skeletal dysplasia. In addition, HS and DS accumulation were found to impair BMP-4 signaling in multipotent adult progenitor cells derived from MPS I patients [27].

The presence of the IDUA transgene in synovium and liver at two-week postinjection prompts an interesting inference. Some amount of intra-articular delivered AAV9-IDUA vector likely escapes the joint space into the bloodstream to transduce hepatocytes and other body tissues, which lead to secretion of enzyme into the bloodstream. This suggests the potential utility of intra-articular gene replacement therapy to generate sufficient blood IDUA to treat other multisystemic MPS I pathologies; however, the study was not designed to assess effects of treatment upon either CNS or visceral disease manifestations.

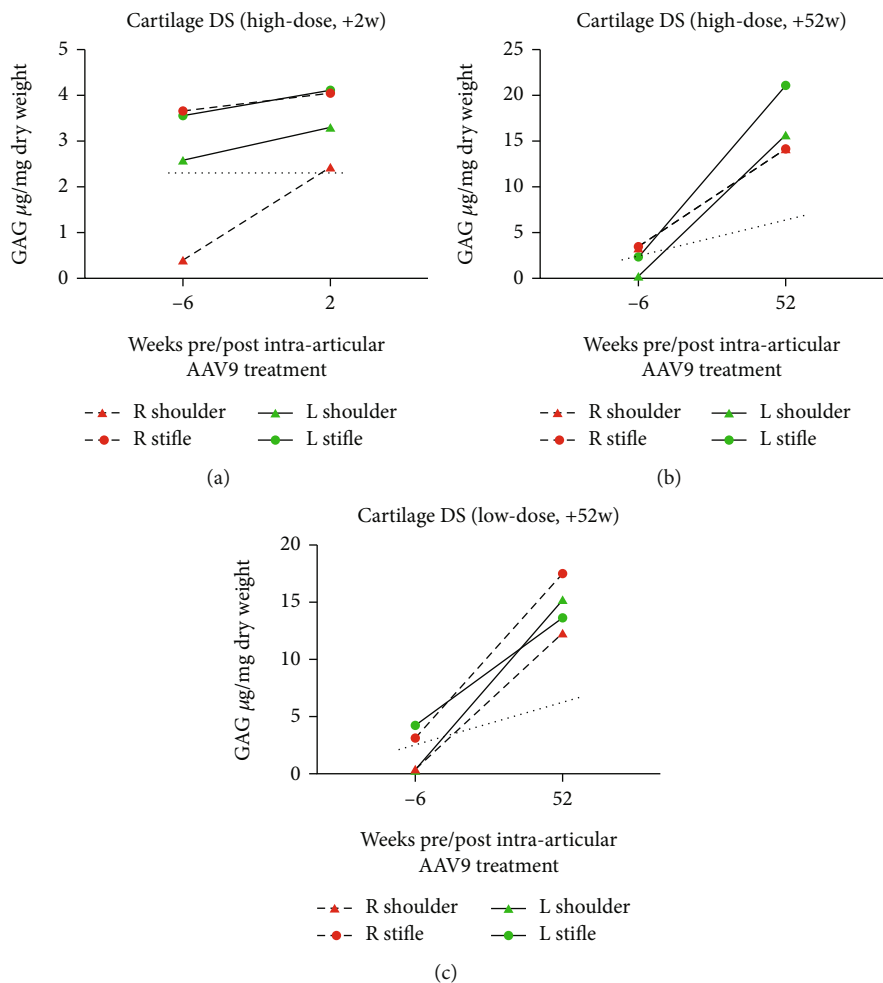


FIGURE 9: Cartilage DS levels in the (a) high-dose +2 w, (b) high-dose +52 w, and (c) low-dose +52 w animals. Cartilage DS levels in all treated animals were greater at necropsy than baseline. Only DS from the AAV9-*IDUA* shoulder of the high-dose +2w animal was comparable to wild-type cartilage.

The findings in the animals necropsied 52-week post-treatment identify challenges to an approach centered solely around intra-articular gene replacement therapy for MPS I. Animals treated at either 5E11 or 5E12 vg/joint doses continued to synthesize synovial IDUA enzyme, albeit slightly above wild-type levels. Shoulder cartilage IDUA in the high-dose +52 w animal was 33% of wild-type; strangely, the *IDUA* transgene was repeatedly observed only in chondrocytes of this animal but not in the synovium. This corresponded to some treatment effect, as shoulder and stifle synovial vacuolization were mild in the high-dose +52-week animal. Regardless, these subnormal/normal IDUA levels were unable to clear substrate; synovial and cartilage GAG levels in AAV9-*IDUA*-treated joints were equivalent to AAV9-*eGFP*-treated joints and markedly elevated compared to normal tissues. Cellular vacuolization was severe in chondrocytes of both animals.

Another important caveat to this proof-of-principle study is that MPS arthropathy affects all joints of the body; we focused gene replacement upon a small number of large joints in these animals. Safe gene replacement of every MPS-affected joint will be a challenge owing to the poten-

tially large vector dosages required, and instead may need to focus upon joints at greatest risk for degeneration (hips) or joints with greatest impact upon daily function (shoulders, knees).

The presence of an anti-IDUA immune response may be one explanation for the lack of clinical efficacy in the older animals. The MPS I canine model is well known to develop a strong antibody response to either intravenously administered or AAV-transduced IDUA protein [28, 29]. Anti-IDUA antibodies are well described in both canine and murine MPS I models to inhibit enzymatic activity and divert enzyme trafficking to nonlysosomal compartments [29, 30]. Anti-IDUA antibodies were found in synovial fluid of both AAV9-*IDUA*- and AAV9-*eGFP*-treated joints, indicating that inhibitory antibodies can cross joint capsules. Alternatively, as some studies have shown, neonatally delivered transgene may become lost, especially in rapidly-dividing tissues [31]. In the two +52-week animals, IDUA enzyme was undetectable in serum and liver, which corresponded to a rapid increase in anti-IDUA serologies and concomitant diminution of IDUA enzyme in blood; IDUA transgene was absent from liver at necropsy. These factors

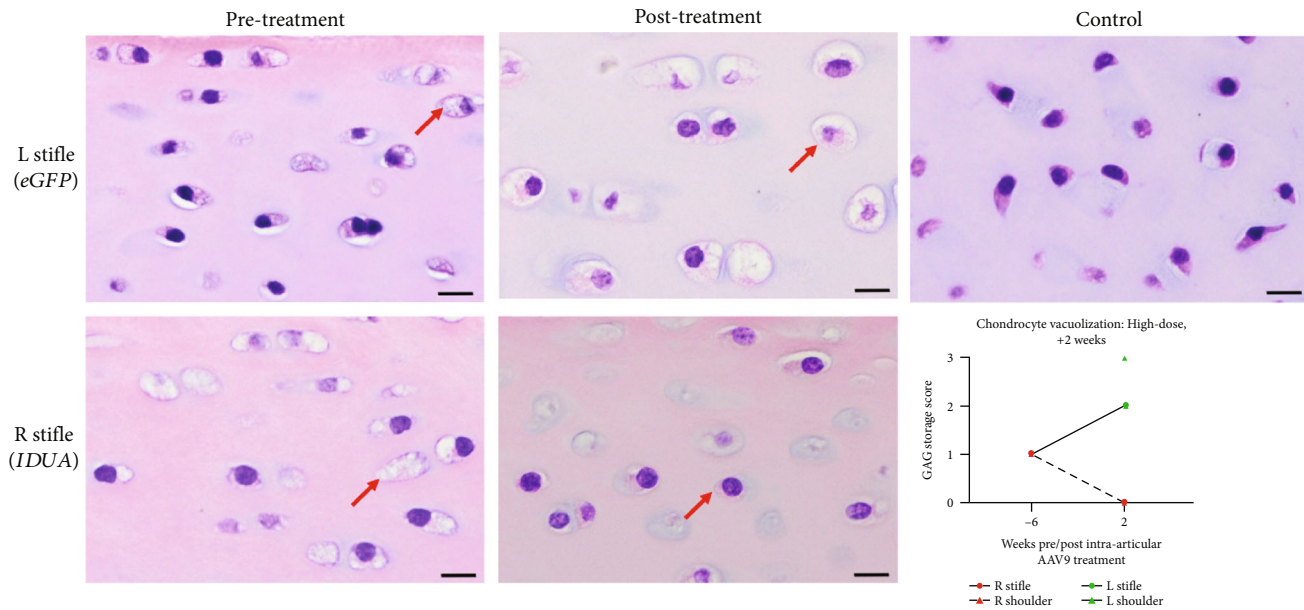


FIGURE 10: Cartilage photomicrographs and chondrocyte lysosomal storage scoring in the high-dose +2 w animal. At baseline, chondrocytes demonstrate foamy lysosomal storage (red arrows, scored 1). At necropsy, AAV9-*eGFP*-treated chondrocytes had increased lysosomal storage (scored 2 or 3), while AAV9-*IDUA*-treated chondrocytes demonstrated normal-appearing basophilic cytoplasm (scored 0). Control chondrocytes included for comparison. Bar = 10 μ M.

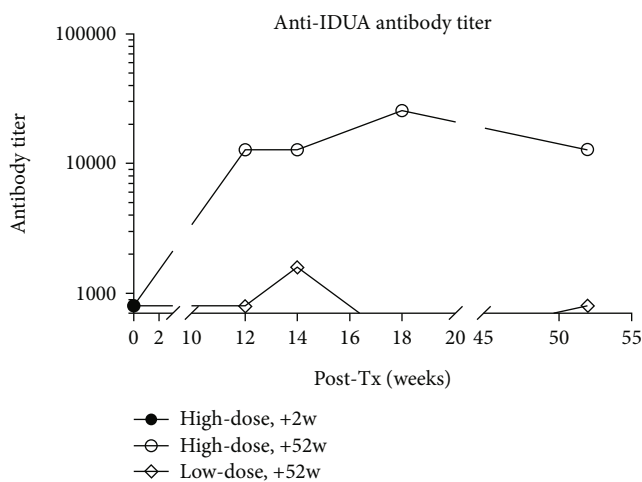


FIGURE 11: Serum anti-*IDUA* antibody levels. All animals had no anti-*IDUA* antibody at baseline. The high-dose +52 w animal demonstrated extremely high anti-*IDUA* serologies, while the low-dose +52 w animal did have detectable but very low anti-*IDUA* antibody levels.

are all potential etiologies for lack of clinical efficacy upon MPS I joint pathology in either +52-week animal.

Additional canine studies to explore the intra-articular route for MPS I therapy are planned; pups will be tolerized with a 5E12 vg/kg intravenous dosage of IV AAV8-*IDUA*, which has been documented to abrogate anti-*IDUA* immune response without cross-reactivity to subsequent AAV9-*IDUA* dosing [29]. As tolerized canines in this previous study expressed supraphysiologic CNS enzyme activity levels until

the time of necropsy at 11 months of age, our follow-up studies will allow for assessment of sustained, high-level intra-articular enzyme synthesis with planned efficacy measures involving joint pathology utilizing ultrasound, magnetic resonance imaging, and other techniques [32]. Enzyme-linked immunosorbent spot assays will be performed to assess cellular immune response to both AAV capsid and *IDUA* protein following treatment. Concurrent intravenous and/or intracerebral *IDUA* gene replacement will also be explored to determine whether the other multisystemic manifestations of MPS I disease can be ameliorated. These studies will assess the feasibility of a multimodal, combination gene replacement therapy approach to address all manifestations of MPS I disease.

Data Availability

The molecular, enzymatic assay, glycosaminoglycan quantitation, serology, and histopathology data used to support the findings of this study are available from the corresponding author upon reasonable request.

Disclosure

N. Matthew Ellinwood's current address is National MPS Society, Durham 27709, USA.

Conflicts of Interest

RYW has no conflicts directly pertinent to the conduct of this study, having received research support from BioMarin and Ultragenyx, served as a consultant for Denali and Takeda, received travel support from Lysogene and

REGENXBIO, and has equity ownership in BioMarin. SK, HZ, JDS, AA, ES, JKJ, and SPY declare that they have no conflict of interest regarding the publication of this paper. PID received research support from Sanofi, M6P Therapeutics, and Alnylam and served as a consultant for Mandos. NME is the employee of the National MPS Society.

Authors' Contributions

All authors state their participation in all four characteristics of authorship including conception or design of the study or acquisition, analysis, interpretation of data for the work, drafting the manuscript and/or revising it critically for important intellectual content, final approval of the version to be published, and agreement to be accountable for all aspects of the work in ensuring that questions related to accuracy or integrity of any part are appropriately investigated and resolved.

Acknowledgments

This study was supported by the University of Pennsylvania Orphan Disease Center Award (MPSI-16-006-01) (RYW, SK, AA, NME, LS, JKJ, HZ, and SPY), the National Institute of Neurological Disorders and Stroke of the National Institutes of Health under award number R01NS085381 (PID, NME), the LifeRay Foundation (RYW), and the Campbell Foundation of Caring (RYW, SK). The content is solely the responsibility of the authors and does not necessarily represent the official views of the NIH. We are grateful for the University of Pennsylvania Vector Core, who provided the AAV9-*eGFP* and AAV9-*IDUA* utilized in this study. We thank the animal care and veterinary staff of the Iowa State University Laboratory Animal Resource and the many undergraduates for enriching the lives and providing excellent and compassionate care of the study animals utilized for this study. Additionally, we would like to thank the Iowa State University College of Agriculture and Life Sciences, the Iowa State University College of Veterinary Medicine, and the State of Iowa. Finally, I am grateful to Pibby, who accompanied me throughout the pandemic and the wee hours of the night writing this manuscript.

Supplementary Materials

Figure S1: synovial transgene and native *IDUA* PCRs. Figure S2: synovial lysosomal storage scoring. Figure S3: chondrocyte lysosomal storage scoring. (*Supplementary Materials*)

References

- [1] E. F. Neufeld and J. Muenzer, "The mucopolysaccharidoses," in *The Online Metabolic and Molecular Bases of Inherited Disease*, D. Valle, S. Antonarakis, A. Ballabio, A. Beaudet, and G. A. Mitchell, Eds., McGraw-Hill Education, New York, NY, 2019.
- [2] S. Verheyen, J. Blatterer, M. R. Speicher et al., "Novel subtype of mucopolysaccharidosis caused by arylsulfatase K (ARSK) deficiency," *Journal of Medical Genetics*, vol. 59, no. 10, pp. 957–964, 2022.
- [3] J. Muenzer, J. E. Wraith, L. A. Clarke, and the International Consensus Panel on the Management and Treatment of Mucopolysaccharidosis I, "Mucopolysaccharidosis I: management and treatment guidelines," *Pediatrics*, vol. 123, no. 1, pp. 19–29, 2009.
- [4] Z. Jiang, S. Byers, M. L. Casal, and L. J. Smith, "Failures of endochondral ossification in the mucopolysaccharidoses," *Current Osteoporosis Reports*, vol. 18, no. 6, pp. 759–773, 2020.
- [5] K. K. White and T. Sousa, "Mucopolysaccharide disorders in orthopaedic surgery," *The Journal of the American Academy of Orthopaedic Surgeons*, vol. 21, no. 1, pp. 12–22, 2013.
- [6] L. A. Clarke, J. E. Wraith, M. Beck et al., "Long-term efficacy and safety of laronidase in the treatment of mucopolysaccharidosis I," *Pediatrics*, vol. 123, no. 1, pp. 229–240, 2009.
- [7] M. Aldenhoven, S. A. Jones, D. Bonney et al., "Hematopoietic cell transplantation for mucopolysaccharidosis patients is safe and effective: results after implementation of international guidelines," *Biology of Blood and Marrow Transplantation*, vol. 21, no. 6, pp. 1106–1109, 2015.
- [8] R. M. Shull, N. E. Hastings, R. R. Selcer et al., "Bone marrow transplantation in canine mucopolysaccharidosis I. effects within the central nervous system," *The Journal of Clinical Investigation*, vol. 79, no. 2, pp. 435–443, 1987.
- [9] M. A. Breider, R. M. Shull, and G. Constantopoulos, "Long-term effects of bone marrow transplantation in dogs with mucopolysaccharidosis I," *The American Journal of Pathology*, vol. 134, no. 3, pp. 677–692, 1989.
- [10] E. D. Kakkis, M. F. McEntee, A. Schmidtchen et al., "Long-term and high-dose trials of enzyme replacement therapy in the canine model of mucopolysaccharidosis I," *Biochemical and Molecular Medicine*, vol. 58, no. 2, pp. 156–167, 1996.
- [11] J. E. Wraith, "Limitations of enzyme replacement therapy: current and future," *Journal of Inherited Metabolic Disease*, vol. 29, no. 2-3, pp. 442–447, 2006.
- [12] M. Aldenhoven, R. F. Wynn, P. J. Orchard et al., "Long-term outcome of hurler syndrome patients after hematopoietic cell transplantation: an international multicenter study," *Blood*, vol. 125, no. 13, pp. 2164–2172, 2015.
- [13] R. Walker, K. G. Belani, E. A. Braunlin et al., "Anaesthesia and airway management in mucopolysaccharidosis," *Journal of Inherited Metabolic Disease*, vol. 36, no. 2, pp. 211–219, 2013.
- [14] J. Hordeaux, C. Hinderer, E. L. Buza et al., "Safe and sustained expression of human iduronidase after intrathecal administration of adeno-associated virus serotype 9 in infant rhesus monkeys," *Human Gene Therapy*, vol. 30, no. 8, pp. 957–966, 2019.
- [15] S. Marcó, V. Haurigot, M. L. Jaén et al., "Seven-year follow-up of durability and safety of AAV CNS gene therapy for a lysosomal storage disorder in a large animal," *Molecular Therapy-Methods & Clinical Development*, vol. 23, pp. 370–389, 2021.
- [16] R. Y. Wang, A. Aminian, M. F. McEntee et al., "Intra-articular enzyme replacement therapy with rhIDUA is safe, well-tolerated, and reduces articular GAG storage in the canine model of mucopolysaccharidosis type I," *Molecular Genetics and Metabolism*, vol. 112, no. 4, pp. 286–293, 2014.
- [17] C. H. Vite, I. Nestrasil, A. Mlikotic et al., "Features of brain MRI in dogs with treated and untreated mucopolysaccharidosis type I," *Comparative Medicine*, vol. 63, no. 2, pp. 163–173, 2013.
- [18] L. Wang, R. Calcedo, P. Bell et al., "Impact of pre-existing immunity on gene transfer to nonhuman primate liver with

- adeno-associated virus 8 vectors,” *Human Gene Therapy*, vol. 22, no. 11, pp. 1389–1401, 2011.
- [19] H. Zhang, S. P. Young, C. Auray-Blais, P. J. Orchard, J. Tolar, and D. S. Millington, “Analysis of glycosaminoglycans in cerebrospinal fluid from patients with mucopolysaccharidoses by isotope-dilution ultra-performance liquid chromatography-tandem mass spectrometry,” *Clinical Chemistry*, vol. 57, no. 7, pp. 1005–1012, 2011.
- [20] A. M. Traas, P. Wang, X. Ma et al., “Correction of clinical manifestations of canine mucopolysaccharidosis I with neonatal retroviral vector gene therapy,” *Molecular Therapy*, vol. 15, no. 8, pp. 1423–1431, 2007.
- [21] R. S. Herati, V. W. Knox, P. O'Donnell, M. D'Angelo, M. E. Haskins, and K. P. Ponder, “Radiographic evaluation of bones and joints in mucopolysaccharidosis I and VII dogs after neonatal gene therapy,” *Molecular Genetics and Metabolism*, vol. 95, no. 3, pp. 142–151, 2008.
- [22] B. Gentner, F. Tucci, S. Galimberti et al., “Hematopoietic stem and progenitor-cell gene therapy for hurler syndrome,” *The New England Journal of Medicine*, vol. 385, no. 21, pp. 1929–1940, 2021.
- [23] J. Bidone, R. S. Schuh, M. Farinon et al., “Intra-articular non-viral gene therapy in mucopolysaccharidosis I mice,” *International Journal of Pharmaceutics*, vol. 548, no. 1, pp. 151–158, 2018.
- [24] E. H. Schuchman and R. J. Desnick, “Mucopolysaccharidosis type I subtypes. Presence of immunologically cross-reactive material and in vitro enhancement of the residual alpha-L-iduronidase activities,” *The Journal of Clinical Investigation*, vol. 81, no. 1, pp. 98–105, 1988.
- [25] G. B. Johnson, G. J. Brunn, Y. Kodaira, and J. L. Platt, “Receptor-mediated monitoring of tissue well-being via detection of soluble heparan sulfate by toll-like receptor 4,” *Journal of Immunology*, vol. 168, no. 10, pp. 5233–5239, 2002.
- [26] C. M. Simonaro, “Cartilage and chondrocyte pathology in the mucopolysaccharidoses: the role of glycosaminoglycan-mediated inflammation,” *Journal of Pediatric Rehabilitation Medicine*, vol. 3, no. 2, pp. 85–88, 2010.
- [27] S. A. Khan, M. S. Nelson, C. Pan, P. M. Gaffney, and P. Gupta, “Endogenous heparan sulfate and heparin modulate bone morphogenetic protein-4 signaling and activity,” *American Journal of Physiology. Cell Physiology*, vol. 294, no. 6, pp. C1387–C1397, 2008.
- [28] P. Dickson, M. Peinovich, M. McEntee et al., “Immune tolerance improves the efficacy of enzyme replacement therapy in canine mucopolysaccharidosis I,” *The Journal of Clinical Investigation*, vol. 118, no. 8, pp. 2868–2876, 2008.
- [29] C. Hinderer, P. Bell, J. P. Louboutin et al., “Neonatal systemic AAV induces tolerance to CNS gene therapy in MPS I dogs and nonhuman primates,” *Molecular Therapy*, vol. 23, no. 8, pp. 1298–1307, 2015.
- [30] S. Q. Le, S. H. Kan, D. Clarke et al., “A humoral immune response alters the distribution of enzyme replacement therapy in murine Mucopolysaccharidosis type I,” *Molecular Therapy-Methods & Clinical Development*, vol. 8, pp. 42–51, 2018.
- [31] S. O. Han, S. Li, A. McCall et al., “Comparisons of infant and adult mice reveal age effects for liver depot gene therapy in Pompe disease,” *Molecular Therapy-Methods & Clinical Development*, vol. 17, pp. 133–142, 2020.
- [32] R. Gawri, Y. K. Lau, G. Lin et al., “Dose-dependent effects of enzyme replacement therapy on skeletal disease progression in mucopolysaccharidosis VII dogs,” *Molecular Therapy-Methods & Clinical Development*, vol. 28, pp. 12–26, 2023.